Catalytic methane combustion in plate-type microreactors with different channel configurations

He, Li; Fan, Yilin; Bellettre, Jerome; Yue, Jun; Luo, Lingai

Published in:
Chemical Engineering Science

DOI:
10.1016/j.ces.2021.116517

Publication date:
2021

Chemical Engineering Science 236 (2021) 116517

Contents lists available at ScienceDirect

Chemical Engineering Science

journal homepage: www.elsevier.com/locate/ces

Catalytic methane combustion in plate-type microreactors with different channel configurations: An experimental study

Li He [a,b], Yilin Fan [a], Jérôme Bellettre [a], Jun Yue [b,*], Lingai Luo [a,*]

[a] Université de Nantes, CNRS, Laboratoire de thermique et énergie de Nantes, LTeN, UMR 6607, F-44000 Nantes, France
[b] Department of Chemical Engineering, Engineering and Technology Institute Groningen, University of Groningen, 9747 AG Groningen, the Netherlands

HIGHLIGHTS

- Six channel geometries of microreactor were tested for catalytic methane combustion.
- An optimal catalyst specific loading rendered the highest methane conversion.
- Usage of coating, flow distribution uniformity and residence time are key factors.
- Hysteresis effect contributed to maintain the high methane conversion.
- Design guidelines on the channel geometry in microreactors for the CMC are provided.

GRAPHICAL ABSTRACT

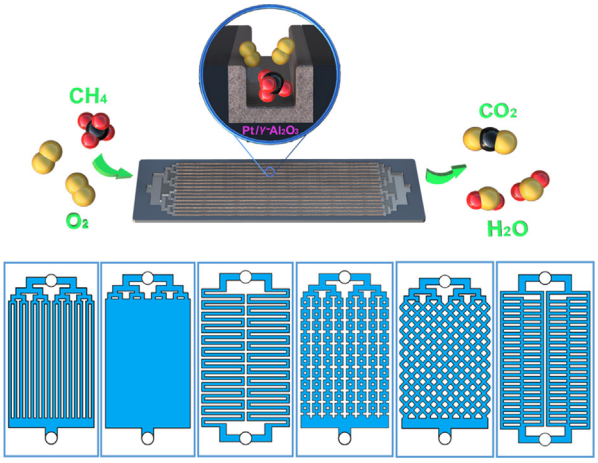

ARTICLE INFO

Article history:
Received 5 November 2020
Received in revised form 4 February 2021
Accepted 5 February 2021
Available online 14 February 2021

Keywords:
Catalytic methane combustion
Microreactor
Washcoated catalyst
Channel configuration
Methane conversion
Flow distribution

ABSTRACT

This paper presents an experimental study on the catalytic methane combustion (CMC) in plate-type microreactors with wall-coated Pt/γ-Al_2O_3 catalyst. Firstly, the influence of different operational conditions and coating properties on the CMC in the straight parallel-channel microreactor has been investigated. A specific catalyst loading of 57.6 g m^{-2} was found to yield the highest methane conversion over 3.5 wt% Pt/γ-Al_2O_3. A higher or lower loading tended to decrease the methane conversion due to either the limited internal diffusion through the thicker coating layer or insufficient active sites in the thinner coating layer. Then, the above microreactor was compared with other five different geometries, including cavity, double serpentine microchannels, obstacled microchannels, meshed circuit and vascular network. The double serpentine microchannel geometry presented the highest methane conversion (especially at a relatively low mixture flow rate) due to the appropriate control over the residence time and catalyst coating surface area.

1. Introduction

Natural gas has been reported to have a largest increment in consumption in the past decade, accounting for nearly half of the increase in global energy demand in year 2018 (Zou et al., 2016; Karavalakis et al., 2012). The combustion of natural gas presents a particular advantage of higher energy content per CO_2 emission (55.7 kJ g^{-1} if fully based on methane as its main component) than coal (39.3 kJ g^{-1}) and petroleum (43.6 kJ g^{-1}), a character which is essential to a low carbon future. In addition to the abundant

* Corresponding authors.
E-mail addresses: yue.jun@rug.nl (J. Yue), lingai.luo@univ-nantes.fr (L. Luo).

https://doi.org/10.1016/j.ces.2021.116517
0009-2509/

Nomenclature

A	Total cross-sectional area of the reaction microchannel in a microreactor, m^2
$F_{CH_4,i}$	Inlet molar flow rate of CH_4, mol s^{-1}
$F_{CH_4,o}$	Outlet molar flow rate of CH_4, mol s^{-1}
$F_{CO_x,o}$	Outlet molar flow rate of CO or CO_2, mol s^{-1}
$F_{H_2,o}$	Outlet molar flow rate of H_2, mol s^{-1}
h	Channel height, m
$l_{j,tot}$	Total channel length between bifurcation indices j and $j+1$, m
$l_{j,1}$	Length of horizontal channel at the index j in the tree-like bifurcated structure, m
Q_{tot}	Total volumetric flow rate, m^3 s^{-1}
r	Ratio of channel width of the downstream to that of the upstream in one bifurcation, -
S	Inner surface area of microchannels subjected to Pt/γ-Al_2O_3 coating, m^2
S_{H_2}	Selectivity of H_2, %
S_{CO_x}	Selectivity of CO or CO_2, %
U	Mean velocity of methane-air mixture in the reaction microchannel, m s^{-1}
V_{tot}	Total microchannel volume for reaction in a microreactor, m^3
W_{cat}	Catalyst mass, g
w_j	Channel width at the index j in the tree-like bifurcated structure, m
X_{CH_4}	CH_4 conversion, %
τ	Mean residence time, s
Φ	Inlet molar ratio of oxygen to methane, -
φ	Specific catalyst loading, g m^{-2}
μ	Dynamic viscosity, Pa s
ρ	Density, kg m^{-3}

Abbreviation

CMC	Catalytic methane combustion
GC	Gas chromatography
i.d.	Inner diameter
MW	Molecular weight
o.d.	Outer diameter
PVA	Polyvinyl alcohol

natural gas reserves proven worldwide, biomethane could be obtained from organic wastes and residues by biomass gasification/digestion (Mehrpooya et al., 2018; Ahmad et al., 2018), providing a competitive energy supply towards a more electrified world. As a result, natural gas has been suggested as a substitute for oil and coal as a future leading energy source for the next 20 years (Gielen, 2018). According to the International Renewable Energy Agency (IRENA) (Gielen, 2018), the utilization of petroleum and coal would decline by 70% and 85%, respectively, by 2050, whereas natural gas would be the largest source by then and achieve peak on its utilization at around 2027 (Gielen, 2018). Thus, a great number of researches have been devoted to the development of energy-efficient natural gas combustion systems in many aspects for their application in the industrial, transport and domestic areas, etc. (Petrov et al., 2018).

However, the gas industry faces some commercial and environmental challenges (Ahmad et al., 2018), due to the releasing of pollutant emissions (e.g., NO_x, CO and unburned hydrocarbon) by the conventional flame combustion of methane typically occurring at above 1400 °C. The harmful impacts of these emissions on the human health and environment have been well recognized (Manisalidis et al., 2020) and the applicable regulations over EU countries have become more and more stringent in recent years. In this context, the catalytic methane combustion (CMC) as a promising alternative has received increasing attention (Chen et al., 2015). A lower working temperature (e.g., <600 °C) is needed for the complete oxidation of methane in the presence of catalyst because of the reduced activation energy (40–80 kJ mol^{-1}) compared to that for conventional combustion (100–200 kJ mol^{-1}). Hence, the exhaust emissions (especially of NO_x) can be remarkably abated (Petrov et al., 2018; Chen et al., 2015; Lee and Trimm, 1995; Farrauto, 2012). Abundant literature is available on the CMC, as summarized by recently published review papers (Chen et al., 2015; Yang and Guo, 2018; Cruellas et al., 2017; He et al., 2019). These existing CMC studies distinguish themselves by focusing on the catalyst development (Farrauto et al., 1992; Wang et al., 2019; Beck et al., 2009; Hwang and Yeh, 1999) and mechanisms (Garbowski et al., 1994; Müller et al., 1999; Ciuparu et al., 2001; Müller et al., 1996; Seimanides and Stoukides, 1986), different types of catalytic reactors (Jodłowski et al., 2017; Seo et al., 2003; O'Connell et al., 2009; Dong et al., 2006; X. Chun, 2005) and (optimized) reaction conditions (Burch and Loader, 1994; Lyubovsky et al., 2003; Wang et al., 2017; Halabi et al., 2010), as well as the target applications (Chun, 2005; Hao et al., 2016; Su and Yu, 2015).

Various types of catalysts have been studied for the CMC including noble metal catalysts and mixed oxides catalysts (perovskites and hexaaluminate) (Chen et al., 2015; Bhagiyalakshmi et al., 2010; Gélin and Primet, 2002). Among them, noble metal catalysts (e.g., Pt, Pd, Rh) are the most commonly used and well developed owing to their high specific surface area, high catalytic activity and low light-off temperature (Burch and Loader, 1994; T.V. Choudhary, 2002). Bimetallic catalysts (e.g., Pd-Pt/Al_2O_3) often show higher catalytic activity and selectivity than their monometallic counterparts due to the synergistic effect by metal–metal interaction (Persson et al., 2007; Persson et al., 2005). Additionally, different supports and additives (e.g., ZrO_2, CeO_2 (Pecchi et al., 2004; Specchia et al., 2009)) have been introduced to improve the catalytic activity through the acceleration of oxygen exchange. In terms of the catalyst form, washcoated catalysts have undergone rapid development in recent years. The washcoated catalyst is commonly deposited as a thin layer on structured surfaces of monolithic reactors or (multichannel) microreactors, in order to avoid the high pressure drop and large temperature gradient likely existing in conventional fixed/packed bed reactors loaded with catalyst powders or pellets (O'Connell et al., 2009). In this regard, the good adhesion and coverage of the coated catalyst layer on the channel walls are essential for the CMC performance of the reactor. The suspension method (Zapf et al., 2003; Peela et al., 2009; Liauw et al., 2000; He et al., 2020) and sol–gel method (Xu et al., 1995; Haas-Santo et al., 2001) are most commonly used for washcoating. It has been reported that the preparation method, binder nature, pH value and particle size could be the key factors that have to be adapted to obtain a high thermal stability and a uniform coverage of the coating (He et al., 2020).

Fixed/packed-bed reactor (with catalysts typically in the form of fine powder) is conventionally employed for the research of the catalyst activity and reaction mechanism due to the easy operation and enhanced catalyst spatial density. Nevertheless, the low surface area, poor temperature uniformity and relatively high pressure drop are main disadvantages of the conventional fixed-bed reactor (He et al., 2019). As an interesting alternative, the microreactors present a high surface-to-volume ratio, relatively low

pressure drop, and high mass/heat transfer rate (especially when combining with washcoat catalyst), which is beneficial to prevent the catalyst sintering in the long term due to the better temperature regulation. As more attention has been paid on the research of microreactors, it could become a promising candidate for potential industrial applications. In particular, plate-type microreactors containing a multitude of microchannels arranged in parallel have attracted great interests (Schmidt and Liauw, 2005; Mills et al., 2007). In combination with the well-adhered catalyst coating on the wall surface, the plate-type multichannel microreactors offer numerous advantages, including the compact design, easy to manufacture and the scaling-up potential to handle a large amount of reactive gas (Ganley et al., 2004a; Ganley et al., 2004b). These features are especially beneficial for handling the CMC or highly exothermic reactions in general by suppressing the presence of temperature hot spots due to the local accumulation of reaction heat (Miesse et al., 2004; Jensen, 2001; Exchangers, 2000). For instance, the experimental study by O'Connell et al. (O'Connell et al., 2009) shows that a 100% conversion could be obtained in a multichannel microreactor (500 μm width × 250 μm depth, 14 channels in total) washcoated with Pt-W or Pt-Mo/γ-Al_2O_3 catalyst at 600 °C and a total gas flow rate of 107 mL min^{-1} (space velocity of 74,000 h^{-1}) and an O_2/CH_4 molar ratio of 2.2. He et al. (He et al., 2020) experimentally performed the CMC in a multichannel reactor (275 mm length × 1.5 width mm × 1 mm height, 32 channels in total) over the washcoated Pt/γ-Al_2O_3 catalyst. A 95.75% methane conversion was obtained at 450 °C under a total gas flow rate of 110 mL min^{-1} (space velocity: 6,557 h^{-1}) and an O_2/CH_4 molar ratio of 2. Moreover, the compact and modular feature of the plate-type multichannel microreactor makes it possible for a better utilization of the reaction heat (Mundhwa et al., 2017; Mundhwa and Thurgood, 2017). The development of the so-called autothermal reactor that combines the CMC (exothermic reaction) with another endothermic reaction (e.g., methane steam reforming to produce hydrogen or syngas) within a single device has become a research hotspot over the past decade (Ramaswamy et al., 2008). Mundhwa et al. (Mundhwa et al., 2017; Mundhwa and Thurgood, 2017) proposed a stacked autothermal reactor design which was composed of two plates with parallel microchannels (5 cm length × 1 mm width, 15 channels, coated with ca. 20 μm thick Pt/Al_2O_3 catalyst) for the CMC and other two plates of cavity shape (5 cm length × 5 cm width × 100 μm depth, with washcoated Ni/Al_2O_3 catalyst) for the methane steam reforming reaction. Their numerical results show that this compact multiple plate design (especially under the co-current mode between flows) could reduce the required amount of catalyst for the CMC by 70% and maintain a uniform temperature profile for the methane steam reforming (Mundhwa et al., 2017; Mundhwa and Thurgood, 2017). The scale-out strategy of microreactor stacks has been investigated numerically for coupling such exothermic and endothermic processes (Mettler et al., 2010). The results illustrate that a certain number of stacks (e.g., >15) was needed so that the released reaction heat could compensate for the heat loss and thus drive the reforming reaction effectively (Mettler et al., 2010).

It is noteworthy that most of the plate-type multichannel microreactors tested for the CMC or simulated for its autothermal coupling have a simple configuration like parallel straight channels (O'Connell et al., 2009; He et al., 2020; Mundhwa et al., 2017; Mundhwa and Thurgood, 2017; Ramaswamy et al., 2008; Mettler et al., 2010; Mei et al., 2007). In this respect, the influence of the operating parameters and the washcoated catalyst properties (e.g., of the promising noble metal-based one) on the CMC performance needs more systematic investigations, as the current understanding is still far from being sufficient. Furthermore, in order to provide an effective way to realize the miniaturization, the design and optimization of microchannel geometries deserve particular attention. On one hand, the improved mixing and the enhanced the mass/heat transfer of appropriate microchannel configurations (compared to parallel straight channel) will render a better reactor performance so that the (nearly) 100% methane conversion could be achieved at a lower temperature or with a lower needed amount of catalysts. The lifetime of noble metal catalysts could be prolonged for a higher cost-effectiveness of the CMC technology. On the other hand, the better thermal management of this strong exothermic reaction achieved by optimizing the reaction channel configuration will facilitate the design of the associated cooling system, which is especially beneficial for various aimed applications such as autothermal reactor and CMC boiler. However, the testing and comparison of different microchannel geometries on the CMC performance have been rarely reported in the literature. There is still much room for the reactor performance improvement by optimizing the internal microchannel configurations that lead to a better process control (e.g., narrowed residence time distribution and more uniform reactant flow distribution) and catalyst utilization (e.g., high catalyst surface area and improved gas–solid mass transfer) in the CMC. Such microreactor performance optimization is equally important towards obtaining a better usage of the released reaction heat from the CMC in energy applications, such as the small-scale water boiler and the autothermal reaction device.

As a continuation of our previous study (He et al., 2020), this work has firstly presented an experimental investigation into the CMC performance over the microreactor with parallel straight channels coated with Pt/γ-Al_2O_3 catalyst. The influence of different operation conditions (e.g., temperature, flow rate and oxygen to methane molar ratio), catalyst loading and thickness, reaction microchannel length was studied. Then, the reaction performance of this type of microreactor was compared with those of other five type of microreactors with different channel configurations. The studied configurations cover some relatively simple channel geometries (cavity and double serpentine microchannels) and more complicated ones (obstacled microchannels, meshed circuit and vascular network). The methane conversion between different microreactor designs has been compared and explained based on the internal channel surface area, residence time and the specific catalyst loading. Moreover, the use of tree-like bifurcation structure for fluid distribution or collection in the microreactor was explored towards improved reaction performance. The findings of this work may help to achieve a flexible and compact design of microreactors that allows upscaling from laboratory to field-scale applications of the CMC with optimized performance.

2. Experimental

2.1. Experimental setup and procedures

The experimental test rig is shown in Fig. 1. Two mass flow controllers (MFC, Brooks SLA5850) were used to adjust the flow rates of methane and the synthetic air for the CMC experiment. The total gas flow rate was adjusted from 110 to 500 mL min^{-1} (based on ca. 20 °C and 1 atm).

For each test, the oven (Nabertherm, LT 9/11/B170) was firstly heated up to the target temperature at a ramp of ca. 15 °C min^{-1} flowing with air to prevent any reaction from happening during heating up process. Once the oven temperature reached the target reaction temperature ranging between 300 °C and 500 °C, the methane-air gas mixture (at an O_2/CH_4 molar ratio from 0.5 to 6) first passed through the inlet pre-heating coil (stainless steel; i.d.: 3.7 mm, o.d.: 6 mm, ca. 20 cm in length) in the oven, and was then introduced into the plate-type microreactor where the

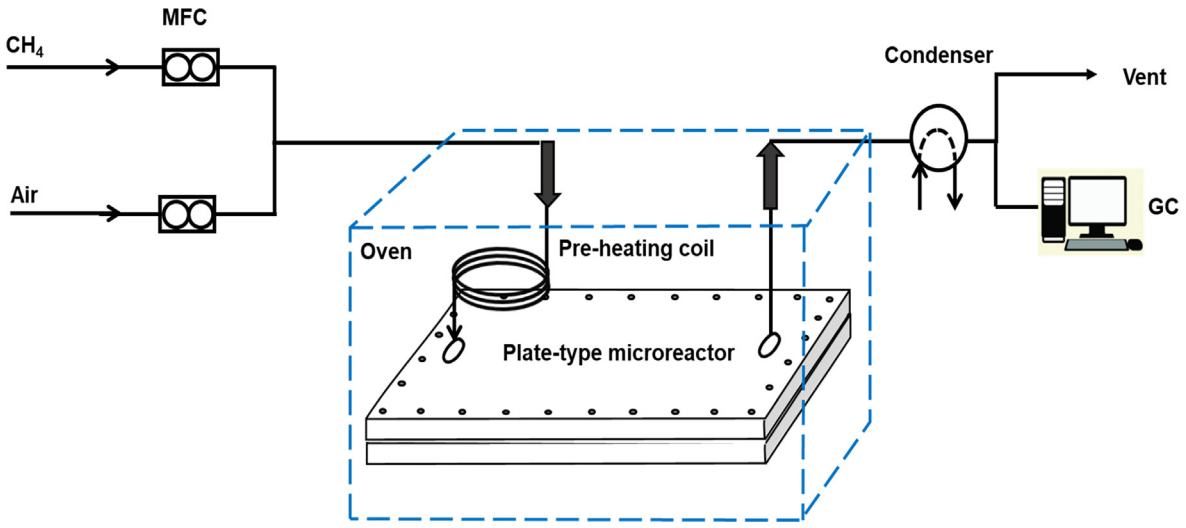

Fig. 1. Test rig for the CMC in the plate-type microreactor.

catalytic reaction happened. The product gas first flew out through a condenser to remove water, and was then analyzed by an online gas chromatography (GC).

2.2. Reactor design and fabrication

The plate-type microreactor has an overall dimension of 190 mm in length, 130 mm in width and 10 mm in height. It was designed as a sandwich shape with a reaction plate (made of FeCrAlloy, i.e., Kanthal A-1, 22% Cr, 5.8% Al and Fe for balance) in the middle, enclosed by two additional blind plates (made of stainless steel) as the outside shell (Fig. 2). One blind plate has additional inlet and outlet ports in order to interface with the reaction platelet (*vide infra*). A graphite gasket (3 mm in thickness) was installed in between these plates to prevent the gas leakage and bolts were used on the peripherals for further sealing. A liquid leak detector (Snoop) was applied on the assembled microreactor in order to ensure the tightness before each series of the test.

The middle reaction plates have an overall dimension of 112.5 mm (length) × 50 mm (width) × 3 mm (height). Each plate has a single inlet port and outlet port (i.d.: 6.5 mm) aligned with the central line, the distance between their centers being 82.5 mm. Six shapes of the internal flow network have been designed and machined on one side of the plate, all of them having a symmetric geometry, as shown in Fig. 2. Each flow network consists of three parts: the inlet distributor, reaction microchannel(s) subjected to the catalyst coating (on two sides and the bottom surface of the microchannel wall) and outlet collector. A detailed description of the six reactors (Reactors #1–6) and its flow network is presented as follows. Note that except for the cavity case (Reactor #2), all the reaction microchannels have a rectangular cross-section of 1.5 mm in width and 1 mm in height.

Reactor #1 (denoted as the straight parallel channel microreactor) has a basic shape of 16 parallelized and straight reaction microchannels of 60 mm in length. The thickness of the separating walls between neighbouring microchannels is 1.5 mm.

Reactor #2 (denoted as the cavity microreactor) has a simple cavity geometry for reaction (dimension: 66.45 mm length × 46.5 mm width × 1.0 mm depth).

Reactor #3 (denoted as the double serpentine channel microreactor) consists of two serpentine reaction microchannels arranged in axial symmetry. For each zigzag unit, the channel length of the horizontal section is 21 mm and that of the vertical section is 4.5 mm, the angle of zigzags being 90°. The thickness of the separating walls is 1.5 mm. The total length of each serpentine microchannel is 547.02 mm.

Reactor #4 (denoted as the obstacled parallel channel microreactor) differs from the basic straight parallel channel microreactor (Reactor #1) by the presence of solid obstacles (square shape, 1.5 mm × 1.5 mm) along the flow direction in the reaction microchannels. Each microchannel thus assumes a split-and-recombine shape around successive obstacles (4.5 mm × 4.5 mm, 10 pieces for each, 80 in total). The thickness of walls separating the microchannels is 1.5 mm. The connection unit between repeating split-and-recombine units is 1.5 mm in length and 1.5 mm in width.

Reactor #5 (denoted as the meshed circuit microreactor) presents a meshed flow circuit with channel interlacing, inspired by the land crack architecture in nature (Tondeur et al., 2011). The reaction microchannels are intersected at a crossing angle of 90°. The solid diamond blocks formed between the adjacent microchannels have a dimension of 2.74 mm × 2.74 mm with 143 pieces in total.

Reactor #6 (denoted as the vascular microreactor) has two vascular blocks arranged in axial symmetry. For each vascular block, there are two side vertical microchannels (69 mm length × 1.5 m m width) for gas splitting whereas one central vertical microchannel (66 mm length × 1.5 mm width) for recombining. The side and central vertical microchannels are connected by means of short horizontal microchannel sections (9 mm length × 1.5 mm width, 86 pieces in total) that are arranged in a staggered pattern and separated by rectangular parallelepipeds (9 mm in length and 1.5 mm in width).

The inlet fluid distributor and outlet fluid collector fed with the reaction microchannel(s) also differ to some extent in Reactors #1–6. The combination of a multi-scale bifurcated distributor and a simple rectangular collector was employed for Reactors #1, 2, 4 and 5 (Fig. 2). Regarding Reactors #3 and 6, the above structures are not very appropriate due to the geometrical constraints, i.e., the reaction microchannel being either limited in number (only two in Reactor #3) or with a special shape (vascular in Reactor #6). Thus, a simple bilateral divergent or convergent channel network was used as the distributor or collector, respectively. The design, scaling relations and detailed dimensions for these distributors/collectors are found in Appendix A.

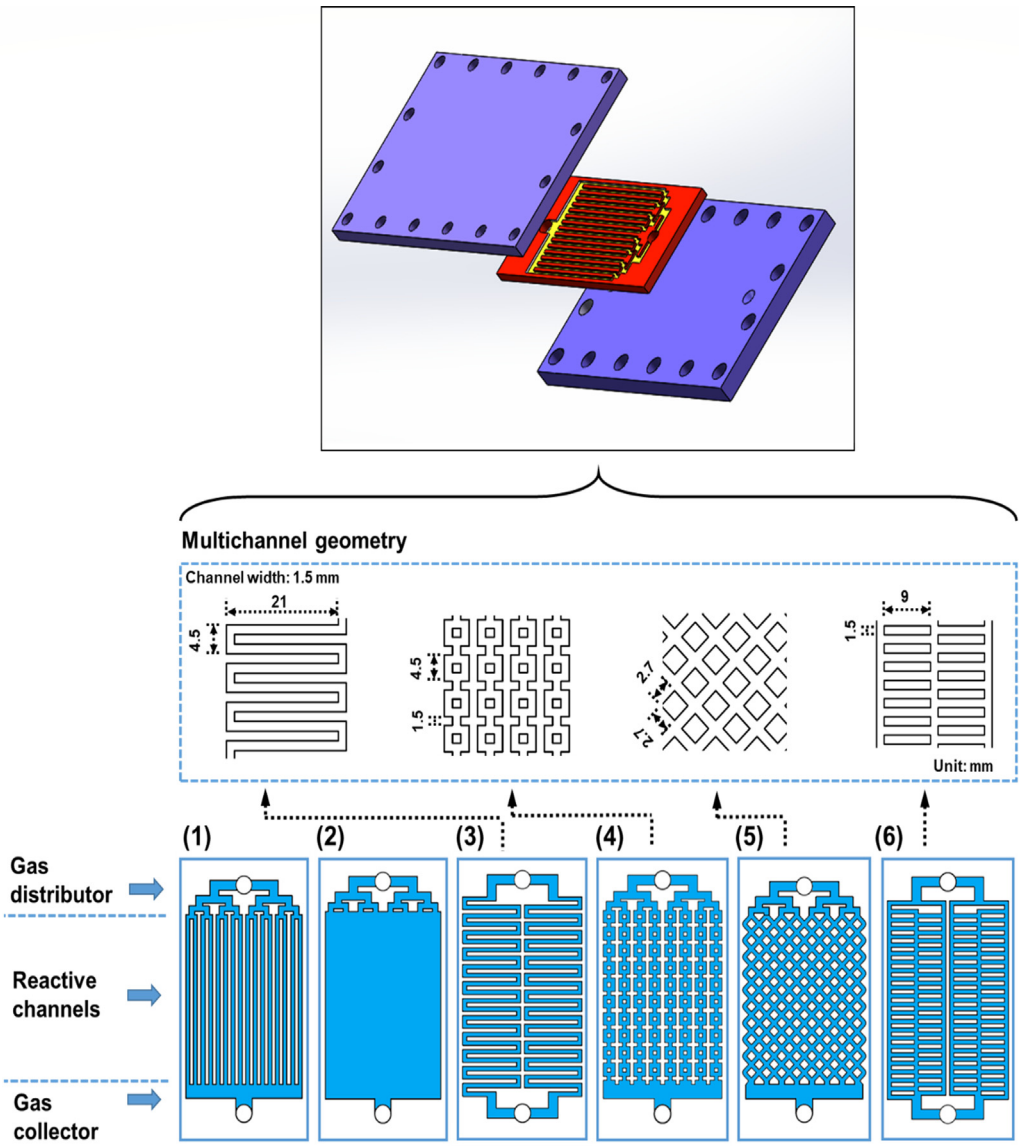

Fig. 2. Schematics of various plate-type microreactors. Reactors #1–6 denote, respectively, the straight parallel channel microreactor, cavity microreactor, double serpentine channel microreactor, obstacled parallel channel microreactor, meshed circuit microreactor and vascular microreactor.

2.3. Catalyst preparation and coating procedures

The reaction platelets were first immersed with acetone at 45 °C for 30 min in the ultrasonic bath (PCE-UC 20) with the frequency being 40 kHz, in order to remove oil, grease and other dirt (Meille et al., 2005). Thermal pretreatment was subsequently performed at 900 °C (ramp from room temperature: 20 °C min^{-1}; 10 h at the final temperature), in order to generate a thin alumina layer over the substrate surface which could be a strong bonding between the Pt/γ-Al_2O_3 coating layer and the substrate.

The slurry suspension method was applied for the coating deposition in microreactors (Giani et al., 2006; Cebollada and Garcia Bordejé, 2009). The materials used for preparing the catalytic coating were as follows: γ-Al_2O_3 (3 μm, 99.97% on metals basis), PVA (98–99% hydrolyzed), acetic acid and tetraammineplatinum (II) nitrate ($Pt(NH_3)_4(NO_3)_2$, 99.99% on metals basis) purchased from Alfa Aesar. The γ-Al_2O_3 slurry was prepared by mixing γ-Al_2O_3 powder, PVA binder and acetic acid (Zapf et al., 2003), based on the optimized composition identified in our previous study (He et al., 2020): 5 wt% PVA (MW of 146,000–186,000), 20 wt% Al_2O_3 (3 μm) and 1 wt% acetic acid. The γ-Al_2O_3 slurry was then heated up to 65 °C for 2 h under 300 rpm stirring and stored at room temperature for at least 2 weeks to remove the bubbles inside the slurry before use.

The prepared slurry as the catalyst support precursor was first deposited on the walls (two sides and bottom) of the reaction microchannels for all Reactors #1 to 6 using syringe injection. The applied slurry weight was adjusted as per the required catalyst specific loading (*vide infra*). The excessive suspension outside the microchannel was immediately removed with a razor blade. The platelets were then dried at room temperature overnight for at least 8 h, subsequently dehydrated at 120 °C for 8 h and finally calcined at 600 °C (ramp from room temperature: 2 °C min^{-1}; 2 h at the final temperature).

The incipient wetness impregnation was performed by manually dropping the $Pt(NH_3)_4(NO_3)_2$ solution with a certain Pt concentration (1.5 wt%, 3.5 wt% or 5 wt%) into the reaction microchannel of the platelet coated with γ-Al_2O_3. The impregnated coating was

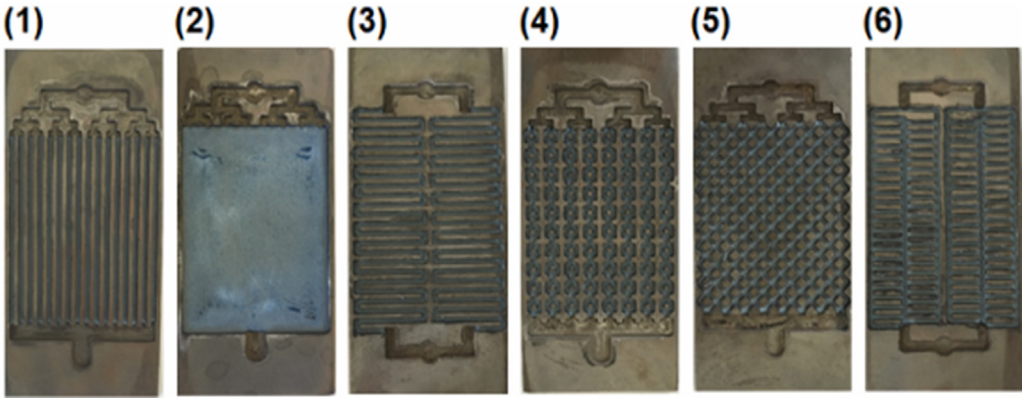

Fig. 3. Reaction platelets coated with Pt/γ-Al_2O_3 catalyst in Reactors #1–6.

then dried at room temperature overnight for at least 8 h, and finally calcined at 500 °C (ramp from room temperature: 2 °C min^{-1}; 2 h at the final temperature). The adhesion of the Pt/γ-Al_2O_3 washcoat catalyst prepared following this procedure has been tested in our previous study by the ultrasonic test and no appreciable weight loss has been found (He et al., 2020). Fig. 3 shows the prepared reaction plates with the coated catalyst. Some geometric parameters of these reactors and the involved Pt/γ-Al_2O_3 catalyst coating characteristics are presented in Table 1. Note that all the area and volume calculations are based on bare microchannels without considering the coating thickness. Based on SEM images from our previous study (He et al., 2020), the coating thickness range is ca. 18 μm (upper parts at side walls) to ca. 110 μm (corner parts), which is much smaller than the microchannel width/height. Given the negligible thickness of catalyst coating (64 μm average) compared with the reaction microchannel width and height, the pressure drop through the reaction microchannel remains almost unaffected by loading the catalyst.

2.4. Analytical procedure

Gas product was analyzed by an online MicroGC (Agilent, R490 OBC) equipped with a thermal conductivity detector. A Molsieve 5 Å column (MS5A, length: 20 m) and a pre-column (PPU, length: 10 m) were used. The concentrations of the reference gas used were 5.12 ± 0.1 mol% CH_4, 2.015 ± 0.04 mol% C_3H_8, 2.024 ± 0.061 mol% C_3H_6, 9.99 ± 0.2 mol% H_2, 9.98 ± 0.2 mol% CO, 1.994 ± 0.04 mol% C_2H_2, 1.999 ± 0.04 mol% n-C_4H_{10}, 2.017 ± 0.04 mol% C_2H_4, 9.92 ± 0.02 mol% CO_2, and N_2 for the rest. Argon was used as the carrier gas. The MicroGC oven temperature was heated from 40 °C up to 100 °C (ramp: 20 °C min^{-1}) and maintained for 7.5 min. SOPRANE II software was used for the peak area integration and data analysis.

2.5. Definitions

The CH_4 conversion (X_{CH_4}), CO_2 (CO) selectivity (S_{CO_x}) and H_2 selectivity (S_{H_2}) are calculated based on Eqs. (1)–(3), respectively.

$$X_{CH_4} = \frac{F_{CH_4,i} - F_{CH_4,o}}{F_{CH_4,i}} \times 100\% \quad (1)$$

$$S_{CO_x} = \frac{F_{CO_x,o}}{F_{CH_4,i} - F_{CH_4,o}} \times 100\% \quad (2)$$

$$S_{H_2} = \frac{F_{H_2,o}}{F_{CH_4,i} - F_{CH_4,o}} \times 100\% \quad (3)$$

where F stands for the molar flow rate (based on ca. 20 °C and 1 atm). The subscripts i and o indicate the inlet and outlet of the plate-type microreactor, respectively.

The mean residence time (τ) is defined as the total void volume of the coated microchannel(s) (V_{tot}) divided by the total volumetric flow rate of the gas mixture entering the reactor (Q_{tot}).

$$\tau = \frac{V_{tot}}{Q_{tot}} \quad (4)$$

The catalyst specific loading φ (unit: g m^{-2}) of the Pt/γ-Al_2O_3 washcoat catalyst deposited on the reaction platelet is calculated as the catalyst mass (W_{cat}) gained on the substrate (i.e., after calcination) divided by the total surface area (S) of the reaction microchannel subject to the coating.

Table 1
Geometric parameters of the tested microreactors and the involved Pt/γ-Al_2O_3 catalyst coating characteristics.

Reactor	S (mm^2)			W_{cat} (g)	φ (g m^{-2})	V_{tot} [c] (mm^3)	τ [d] (s)
	Bottom side [a]	Wall side [b]	Total				
#1	1476.00	1998.02	3474.02	0.27 [e]	78.30 [e]	1476.00	5.90
#2	3089.00	202.88	3291.88	0.25	76.40	3089.00	12.36
#3	1650.06	2200.08	3850.14	0.27	70.26	1650.06	6.60
#4	1620.00	1920.00	3540.00	0.24	67.51	1620.00	6.48
#5	1676.45	1815.26	3491.71	0.24	68.45	1676.45	6.71
#6	2166.00	2249.08	4415.08	0.26	58.28	2166.00	8.66

[a] The surface area of the bottom of the reaction microchannel.
[b] The surface area of two sides walls of the reaction microchannel.
[c] Volume of the reaction microchannel.
[d] Residence time in the reaction microchannel, calculated based on a total gas flow rate of 150 mL min^{-1}.
[e] Other catalyst weights and specific loadings were also tested. Here only the values for comparison with other type of microreactors are shown.

$$\varphi = \frac{W_{cat}}{S} \quad (5)$$

The mean velocity of the gas mixture in the reaction microchannel is defined as the total volumetric flow rate of the gas mixture divided by the total reaction microchannel cross-sectional area (A).

$$U = \frac{Q_{tot}}{A} \quad (6)$$

3. Results and discussion

3.1. CMC performance of the straight parallel channel microreactor

In our previous study (He et al., 2020), the straight parallel channel microreactor of a larger dimension (317.5 mm length × 50 mm width × 3 mm height) with washcoated Pt/γ-Al_2O_3 catalyst has been investigated for the CMC. Therein, the uniformity of γ-Al_2O_3 coating layer at optimized synthesis conditions (pH = 3.5, 5 wt% PVA, 20 wt% γ-Al_2O_3 and particle size being around 3 μm) in the microchannels could be observed from SEM images. Moreover, the catalyst life time test has been performed and the catalyst activity dropped from full conversion to 84.61% at 100 h (He et al., 2020), which could be a reference for the catalyst used in the current study given the same protocol of synthesis. It has been reported that the introduction of promoters/additives (e.g., ZrO_2, CeO_2 (Farrauto et al., 1992; Pecchi et al., 2004; Farrauto et al., 1993)) into the catalyst could effectively prevent the catalyst deactivation by increasing the temperature of thermal decomposition.

In order to gain a deeper understanding of the influence of among others the catalyst loading, thickness, channel length and fluid distribution/collection structure on the methane conversion, the similar type of microreactor, though with a relative smaller dimension (112.5 mm length × 50 mm width × 3 mm height), has been prepared with Pt/γ-Al_2O_3 coating in this work and examined under different reaction conditions.

3.1.1. Effect of the operating conditions

The methane conversion as a function of the reaction temperature (i.e., the oven temperature) under different flow rates at an inlet oxygen to methane molar ratio (Φ) of 2 is shown in Fig. 4. For a given temperature, a higher methane conversion was obtained at a lower flow rate, due to a longer residence time (cf. Eq. (4)). At the beginning when the operating temperature is relatively low (300–350 °C), the methane conversion has no significant difference between different flow rates (150–500 mL min^{-1}). Under such circumstances, the reaction rate is slow and (largely) controlled by kinetics (i.e., predominately determined by the reaction temperature and catalyst mass). Thus, the methane conversion is at a very low level (<3%) and the conversion difference between each flow rate is not very discernible. As the temperature increased, the methane conversion presented a significant increase and the light-off phenomenon occurred. This indicates that the favorable coverage of the adsorbed methane and oxygen over the catalyst surface facilitated by the temperature rise has been reached. Meanwhile, the significant increase in the intrinsic kinetic rate and the catalytic activity during the light-off is likely attributed to the rapid rise of the local temperature as well given the strongly exothermic reaction of methane combustion. The light-off temperature corresponding to a 50% methane conversion (T_{50} value) relevant to conditions in Fig. 4a is shown in Table 2. When the operating temperature continued to increase (e.g., >450 °C), the reaction tended to be (more) governed by mass transfer, because the kinetic rate rapidly increased (according to the Arrhenius equation), but the gas-catalyst mass transfer rate was hardly

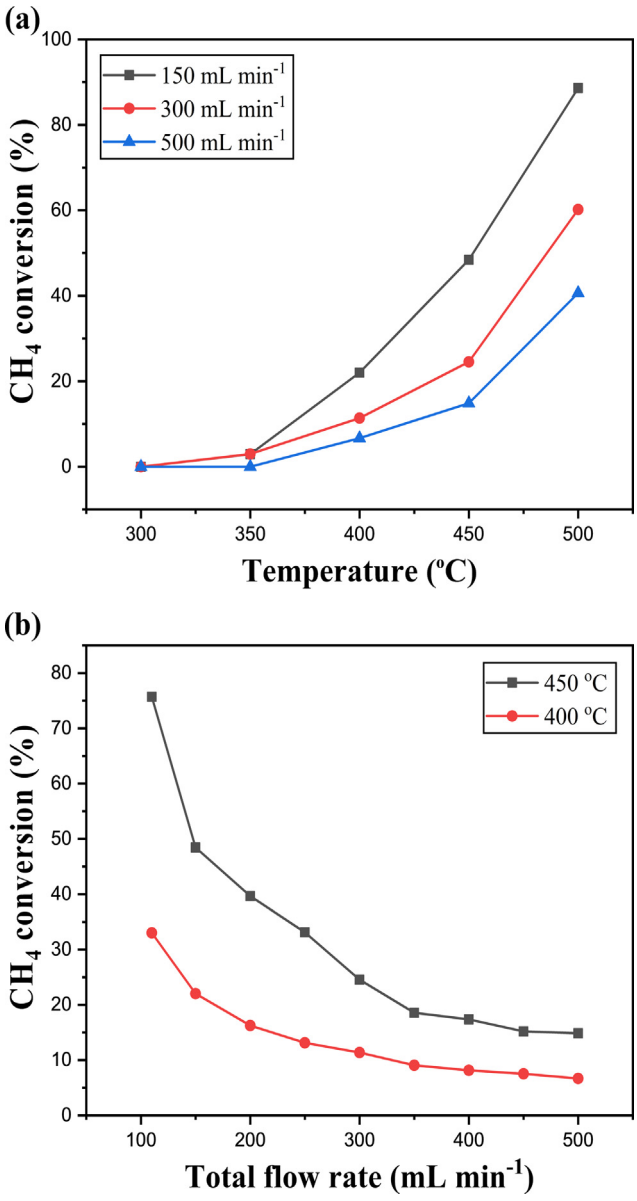

Fig. 4. Methane conversion as a function of (a) the temperature and (b) the total gas flow rate over the washcoated 3.5 wt% Pt/γ-Al_2O_3 catalyst in Reactor #1 (straight parallel channel microreactor). Conditions: T = 300 °C – 500 °C, Φ = 2, Q_{tot} = 110–500 mL min^{-1}.

to catch up with (given much less comparable increase in the species diffusivity in the gas mixture and coating). It is worth noting that the decrement in the methane conversion rendered a slowdown when comparing 150 mL min^{-1} to 300 mL min^{-1} and 300 mL min^{-1} to 500 mL min^{-1} throughout the temperature from ca. 400 to 500 °C. This is in line with T_{50} value difference in Table 2.

Fig. 4b further compares the methane conversion as a function of the flow rate at a given temperature of 400 or 450 °C. The methane conversion presented an obvious decrease with the increasing total flow rate, as already revealed in Fig. 4a. It is worth noting that the decrease in the methane conversion at a sufficiently high flow rate tends to be insignificant. This could be due to the improved external mass transfer at high flow rates which compensate, to some extent, the conversion decrease (due to the shortened residence time). The conversion trends revealed here are in general similar to those for the straight parallel channel microreactor tested in our previous study (He et al., 2020). These results confirm

Table 2
T_{50} value for the CMC experimental data presented in Fig. 4a.

Total flow rate (mL min^{-1})	T_{50}[a,b] (°C)
150	451.8
300	487.6
500	516.0

Note:
[a] T_{50} indicates the temperature for reaching 50% methane conversion; Conditions are shown in Fig. 4a.
[b] Estimated from the polynomial regression line used for fitting the measured conversion curve as a function of the temperature for different flow rates. The polynomial is in the form of $T_{50} = B_0 + B_1 X_{CH_4} + B_2 X_{CH_4}^2$, where B_0, B_1 and B_2 are the fitting constants.

that the coating has been successfully applied onto the current microreactor and functioned well in the CMC.

3.1.2. Effect of catalyst loading and coating thickness

The reaction was further performed at various flow rates in Reactor #1 (straight parallel channel microreactor) with different Pt loadings (1.5 wt%, 3.5 wt% and 5.0 wt% Pt/γ-Al_2O_3) by maintaining almost a constant catalyst weight (W_{cat} = 0.25 ± 0.02 g). In more detail, during the catalyst preparation only the concentration of Pt precursor solution was changed according to the required Pt loading. The obtained results are presented in Fig. 5. At the same total gas flow rate, a higher Pt loading (and with more Pt available in the catalyst) is accompanied by a higher methane conversion. In other words, the overall reaction rate is significantly promoted by the increased kinetic rate at higher Pt loadings. The methane conversion rendered an obvious drop as increasing the total flow rate, due to the reduction of residence time. The extent of such conversion decrease seems more pronounced especially at the highest catalyst loading studied (5.0 wt% Pt/γ-Al_2O_3), indicating that the influence of the external mass transfer was more pronounced therein given the highest kinetic rate involved. Furthermore, the external mass transfer is related to many factors including the flow pattern, the diffusion rate, the channel geometry, etc., by which the reactants have to be transported perpendicularly to the flow direction from the center of microchannel to catalyst external surface (Fogler, 2013). A higher flow rate (or larger Reynolds number) often leads to a higher external mass transfer rate (Fogler, 2013). However, a higher flow rate also tends to incur a lower methane conversion due to the shorter residence time. Thus, the decrement of methane conversion is generally dropped at shortened residence times as presented in Fig. 5.

The internal mass transfer is mainly correlated to catalyst property including the catalyst thickness, tortuosity, porosity and reactant diffusivity, etc. (Fogler, 2013). To further investigate the influence of internal diffusion limitation (if present) on the microreactor performance, the coating thickness of 3.5 wt% Pt/γ-Al_2O_3 catalyst was varied in the experiment by applying different catalyst mass (W_{cat}) onto the reaction microchannel walls in Reactor #1. That is, the higher the W_{cat}, the thicker the coating layer and subsequently the higher the specific catalyst loading φ (Eq. (5)). Microreactors with different values of φ varying from 39.45 to 90.39 g m^{-2} in Reactor #1 have been prepared, and the catalyst layer visually presented a uniform and well-dispersed coating throughout the parallelized reaction microchannels. Fig. 6 illustrates that the methane conversion presents a maximum at about φ = 57.57 g m^{-2} for a given temperature (more clearly seen at above 350 °C) and total flow rate. This phenomenon is probably due to a more or less optimized match between the internal diffusion rate and the intrinsic kinetic rate at φ = 57.57 g m^{-2}. For lower φ values (e.g., 39.45 g m^{-2}), this might be explained by the fact that although the thinner coating layer herein facilitated the internal diffusion due to the shorter path of diffusion, the accompanied insufficient amount of active sites for the reaction (given the Pt weight proportionally decrease in the catalyst) has reduced the methane conversion. For higher φ values (e.g., 78.30 and 90.39 g m^{-2}), the more significant internal diffusion resistance (longer path of diffusion) is likely present due to the increased thickness of the catalyst layer, resulting in a lower methane conversion (despite the higher intrinsic reaction rate due to Pt weight increase in the catalyst based on Arrhenius equation). To be more specific, the higher Thiele modulus and lower effectiveness factor could be obtained at the thicker catalyst coating, suggesting that the effect of internal mass transfer in a thicker coating is more

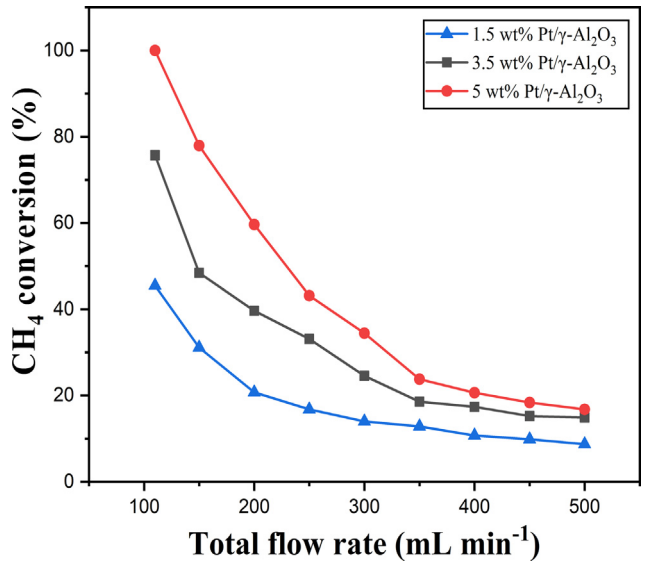

Fig. 5. Methane conversion as a function of the total gas flow rate over different Pt loadings in Reactor #1 (straight parallel channel microreactor). Conditions: T = 450 °C, Φ = 2, Q_{tot} = 110–500 mL min^{-1}, W_{cat} = 0.25 ± 0.02 g.

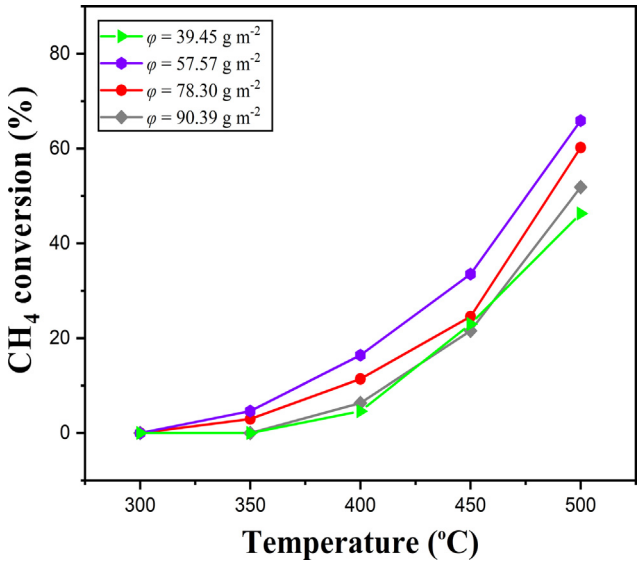

Fig. 6. Methane conversion as a function of the reaction temperature under different specific catalyst loading (φ) in Reactor #1 (straight parallel channel microreactor). Conditions: T = 300–500 °C, Φ = 2, Q_{tot} = 300 mL min^{-1}, 3.5 wt% Pt/γ-Al_2O_3 catalyst.

pronounced on the methane conversion. Thus, φ = 57.57 g m^{-2} is expected to be the optimized compromise between the (internal) mass transfer and instinct kinetics. For a more quantitative prediction of the conversion trend as shown in Fig. 6, a good knowledge on the reaction kinetics and reactant diffusion within the coating layer (which depends primarily on the pore structure and morphology of the coating) needs to be further acquired.

3.1.3. Effect of reaction microchannel length

To gain further insights into the influence of external mass transfer on the reaction rate, the methane conversion in experiments with the straight parallel channel microreactors of different reaction microchannel lengths (50–275 mm) is compared in Fig. 7, where the microchannel width and height are the same. The specific catalyst loading is kept more or less identical (φ = 82.5 ± 5 g m^{-2}). As displayed in Fig. 7, the methane conversion increased with increasing microchannel length at 400 °C for a given mean velocity of the methane-air mixture (U; Eq. (6)). This is logical given the increased residence time in the longer microchannel. A significant increase in the microchannel length (from 60 to 275 mm) did not result in a conversion increase of similar extent. This shows that the reaction is (at least) limited by the external mass transfer, given that under internal diffusion limitation or kinetic control, the overall reaction rate should increase linearly with the catalyst weight applied on the microchannel wall.

As already revealed in Fig. 4b, the methane conversion at a given temperature decreased with the increasing flow rate in the microreactor (Reactor #1), which is insignificant at sufficiently high flow rates (e.g., Q_{tot} = 400 mL min^{-1}; corresponding to a U of 0.28 m/s). The results of Fig. 7 further suggest that at such high Q_{tot} or U values, the methane conversion can be still improved by increasing the microchannel length (translated into a longer residence time). This also implies that if the reaction is operated at a much higher Q_{tot} (than 400 mL min^{-1}) in Fig. 4b, a significant drop in the methane conversion is expected (i.e., the conversion does not level off at such high flow rates).

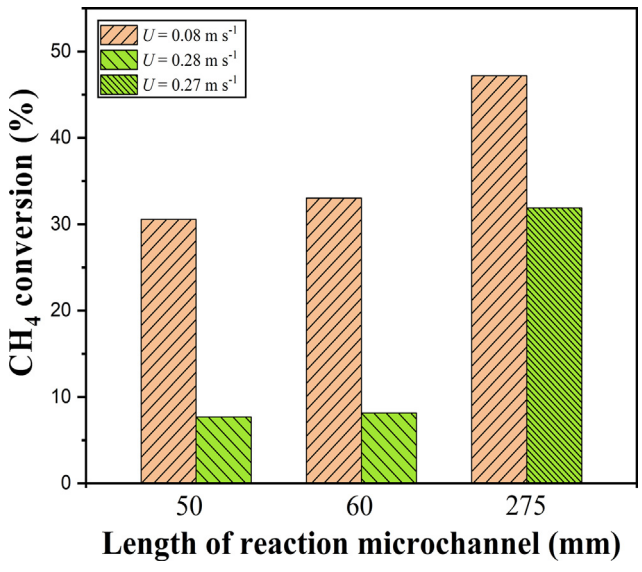

Fig. 7. Methane conversion as a function of the reaction microchannel length at different mixture velocities (U). Conditions: T = 400 °C, Φ = 2, 3.5 wt% Pt/γ-Al_2O_3 catalyst, φ = 81.33, 78.30, and 87.37 g m^{-2} for the microchannel lengths of 50, 60 and 275 mm, respectively, Data for 60 mm microchannel length is based on experiments with Reactor #1 (straight parallel channel microreactor). Data for 50 mm and 275 mm microchannel lengths are from the respective experiments with another microreactor of otherwise the same geometry and the microreactor used in our previous study (He et al., 2020) (but with different numbers of microchannels of the same width/height).

3.1.4. Effect of bifurcated tree-like structure as distributor or collector

The flow distribution behaviour within the reaction microchannel network may have a great impact on the microreactor performance in the CMC. In the experiments performed above in Reactor #1, the bifurcated tree-like structure was used as the inlet fluid distributor whereas a simple rectangular collector at the microchannel outlet (Fig. 2). Regarding the multi-scale tree-like component, its relevant position with respect to the reaction microchannel will influence flow distribution properties, as shown in the previous study (Fan et al., 2008). In order to experimentally verify the influence of such tree-like component on the catalytic performance, additional experiments were performed with Reactor #1, by switching the microreactor outlet and inlet (i.e., by feeding the gas mixture at the microreactor outlet). Thus, the tree-like structure functioned here as the product collector and the rectangular chamber as the fluid distributor.

Fig. 8 presents an interesting observation: for Reactor #1, the tree-like structure used as the outlet product collector exhibited a higher methane conversion than that used as the inlet gas distributor. This indicates a somewhat significant difference in the pressure (drop) between the distributor case and collector case (Fan et al., 2008). When the tree-like structure was used as the gas collector, the pressure drop in the collector side is higher than the case of using the simple rectangular chamber as the collector, and the pressure drop in the distributor side is lower. This means that in the former case, the local pressures at the inlet and outlet of the reaction microchannel are higher than those in the latter case, which is beneficial for a more uniform fluid distribution and thus a better methane conversion. In other words, the lower pressure drop on the distributor side tends to improve the uniform delivery of fluid into each reaction microchannel, and the higher pressure at the reaction microchannel outlet would make the flow therein less affected by the flow behavior within the outlet collector structure. These are also in line with the literature reporting that less vortex was produced and less energy was dissipated when using such tree-like structure as the collector compared with the distributor case (Fan et al., 2008).

Fig. 8 further shows that the conversion improvement in the former case is more pronounced at higher total flow rates. This is possibly because the bifurcated tree-like distributor is shown to

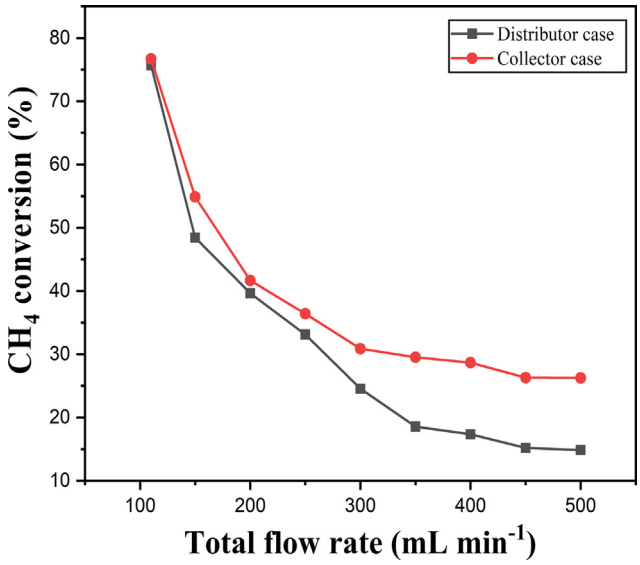

Fig. 8. Influence of the location of the tree-like bifurcated component (i.e., used as the inlet gas distributor or outlet product collector) on the methane conversion in Reactor #1 (parallel straight channel microreactor). Conditions: T = 450 °C, Φ = 2, Q_{tot} = 110–500 mL min^{-1}, 3.5 wt% Pt/γ-Al_2O_3.

be capable of guaranteeing a relatively uniform flow distribution among parallel channels/tubes at small flow rates (Zhou et al., 2018; Guo et al., 2014). Nevertheless, the inevitable flow distribution non-uniformity at high flow rates due to the increasing impact of inertial forces is an intrinsic character of such structure (Zhou et al., 2018). Thus, the tree-like component used as the outlet collector is able to provide a more uniform and stable flow distribution among parallel straight microchannels even under high flow rate conditions. The residence time difference across different reaction microchannels is thereby smaller, leading to a better usage of the catalysts and consequently higher methane conversion.

3.2. Comparison of the CMC performance in microreactors with different internal channel configurations

In the following sub-sections, the CMC performance of Reactor #1 (parallel straight channel microreactor) has been compared with other five plate-type microreactors with different internal channel configurations as shown in Fig. 2, with regard to the effect of the operating temperature, total gas flow rate and molar ratio of O_2 to CH_4 (Φ). In all reactors, the washcoated 3.5 wt% Pt/γ-Al_2O_3 catalyst has the almost identical weight (0.25 ± 0.02 g; Table 1).

3.2.1. Effect of temperature on the performance of different microreactors

The methane conversion as a function of the reaction temperature in different microreactors is shown in Fig. 9a-c for different total flow rates (150–500 mL min^{-1}) and Φ = 2. The same trend as presented in Fig. 4a was observed. At the lower temperature of 300–350 °C, the methane conversion in all Reactors #1–6 is very low (<ca. 5%) and has no obvious difference at different flow rates. This is because the reaction is mainly controlled by kinetics and mass transfer is not the main factor determining the reaction rate. As the temperature increased, the methane conversion presented a significant increase (especially at a lower flow rate), and the light-off phenomenon occurred. An obvious difference in the methane conversion was found among the different channel configurations of Reactors #1–6 at higher temperatures (>ca. 400 °C) when the (external) mass transfer gradually became the limiting factor, especially at a relatively low gas flow rate (e.g., 150 mL min^{-1}; Fig. 9a). At a relatively high flow rate (e.g., 500 mL min^{-1}; Fig. 9c), the gap in the methane conversion between different reactors is narrowed, due to the (largely) improved external mass transfer rate.

With regard to the different channel configurations in microreactors, the methane conversion ranked with the following order: double serpentine channels (Reactor #3) > obstacled straight channels (Reactor #4) > vascular network (Reactor #6) > straight parallel channels (Reactor #1) > cavity (Reactor #2) > meshed circuit (Reactor #5). This trend is more pronounced at a lower total flow rate (e.g., 150 mL min^{-1}; Fig. 9a) and becomes insignificant at higher flow rate (e.g., 500 mL min^{-1}; Fig. 9c). The straight parallel channel microreactor (Reactor #1) presented a higher methane conversion than the cavity microreactor (Reactor #2). The relatively lower methane conversion in Reactor #2 might be due to the negative effect of the non-uniform velocity profile of the gas since only 1 flat cavity was involved (Fig. 2), even though it has the longest mean residence time (cf. Table 1). In other words, the catalyst coating around the cavity experienced different contact times with the reactant mixture, leading to an overall conversion decrease. In contrast, the gas flow distribution should be (much) improved in Reactor #1, given the flow was distributed into 16 parallel straight microchannels contributing to a more uniform contact time between the reactants and catalyst. The obstacle reac-

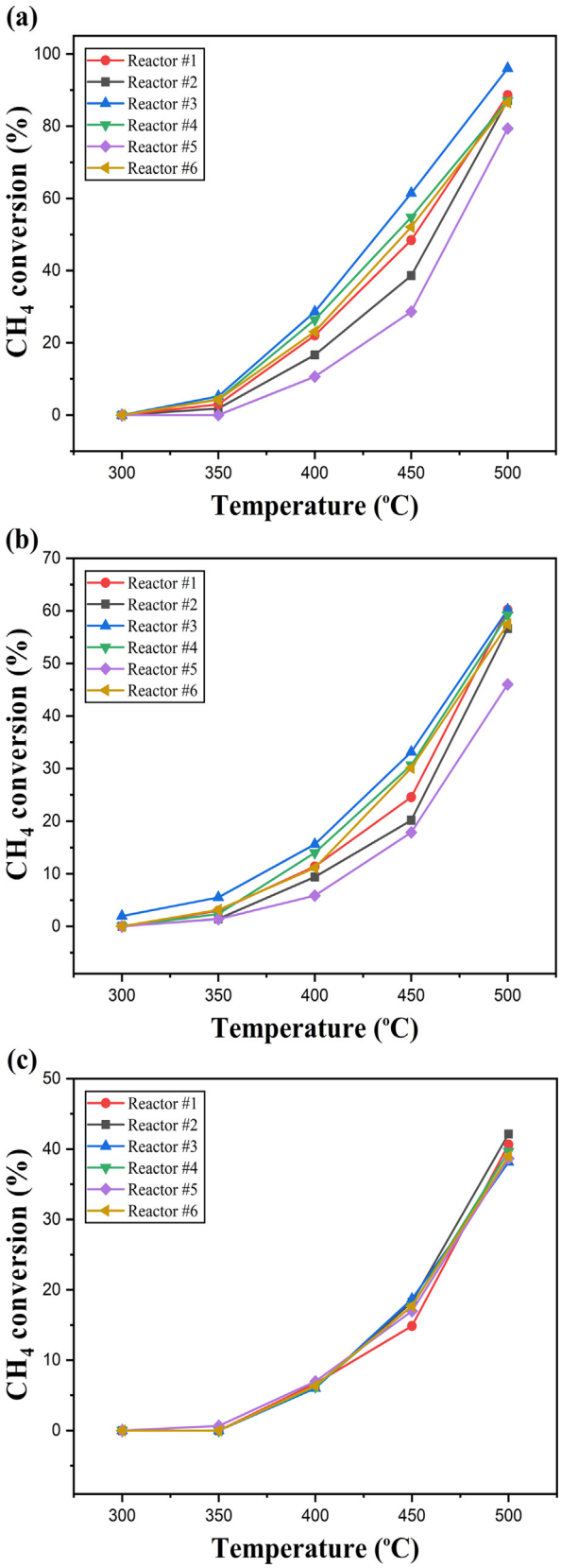

Fig. 9. Methane conversion as a function of the reaction temperature at the total flow rate of (a) 150 mL min^{-1}, (b) 300 mL min^{-1} and (c) 500 mL min^{-1} in plate-type microreactors with different channel configurations (Reactors #1–6). Conditions: T = 300 °C – 500 °C, Φ = 2, 3.5 wt% Pt/γ-Al_2O_3 catalyst. Other reactor details and catalyst properties are shown in Table 1.

tor (Reactor #4) is actually an improved version of Reactor #1, with a slightly higher coating surface area and longer mean residence time (cf. Table 1). Besides, the structure of successive obstacles with the split-and-recombine shape enabled to improve the gas mixing and further enhance the external mass transfer compared to Reactor #1, especially at the mass transfer limited regime (at relatively higher temperatures or low flow rates). It thus offered a slight increase in the methane conversion under the same working conditions compared with Reactor #1. Among all the tested reactors, the highest methane conversion has been achieved by using the double serpentine channel microreactor (Reactor #3). This could be attributed primarily to a relatively higher coating surface area (than all the others except Reactors #6) and relatively longer residence time (than Reactors #1 and 4). In addition, the double serpentine structure could effectively promote the gaseous mixing due to the formation of secondary flow on the channel cross-section (Liu et al., 2000), thus improving their transfer to the coating external surface and contributing to a better conversion. The vascular reactor (Reactor #6) has the highest coating surface area as well as a longer residence time than the other reactors except Reactor #2 (Table 1). Despite these advantages, it presented a methane conversion level in between those of Reactors #4 and 1 (Fig. 9a and b). This is likely due to the non-uniform fluid distribution among the horizontal microchannel sections and thus an insufficient utilization of the coated catalyst. Some microchannels could be overloaded with gas mixture in the vascular network while others were underloaded, which might be related to the vascular structure causing a less uniform distribution of gas mixture. An improved design by carefully adjusting the resistance in the vertical diverging/converging channels may help solve this problem, based on the study of Tondeur et al. (Tondeur et al., 2011). The lowest methane conversion was found in the meshed circuit microreactor (Reactor #5) under the same tested conditions. It has been reported that the flow pattern in the meshed circuit was similar to a continuous stirred tank reactor, and likely tended to be the divergent flow pattern even at low Reynolds numbers (Ni et al., 2005). This indicates that the gas has the chance to flow towards different directions due to divergent flow appeared in the meshed circuit. This probably resulted in the non-uniform flow distribution and/or somewhat broad residence time distribution, and thus a lowest methane conversion.

Among the tested microreactors, the Reactor #3 (double serpentine microchannels) has the highest pressure drop due to the longer channel length and the higher velocity. But its total pressure drop was estimated to be smaller than 0.01 bar under the current experimental conditions (500 mL min^{-1}), lower than that present in fixed/packed bed reactors (e.g., mostly above 0.1 bar (Eigenberger, 2009)) especially when fine catalyst powders are used.

In summary, guidelines regarding the optimal channel configurations in plate-type microreactors for the CMC should comprehensively consider the coating surface area, residence time (distribution), fluid distribution uniformity, and the efficient use of catalyst in order to achieve a desirable methane conversion. Further detailed investigation on the local flow and temperature distribution characteristics by using simulation or optical visualization techniques would help give a clearer view and better understanding in this aspect.

Fig. 10 depicts the methane conversion as a function of the operating temperature at Φ = 6 and a total flow rate of 150 mL min^{-1} in Reactors #1–6. Similar conversion trends and the same microreactor performance ranking were observed as compared to the case of Φ = 2 (Fig. 9a). A lower methane conversion was obtained at Φ = 6 than Φ = 2. A comparison of T_{50} values at Φ = 2 and 6 for different channel configurations is also given in Table 3. It is found that the T_{50} value at Φ = 2 is slightly lower than

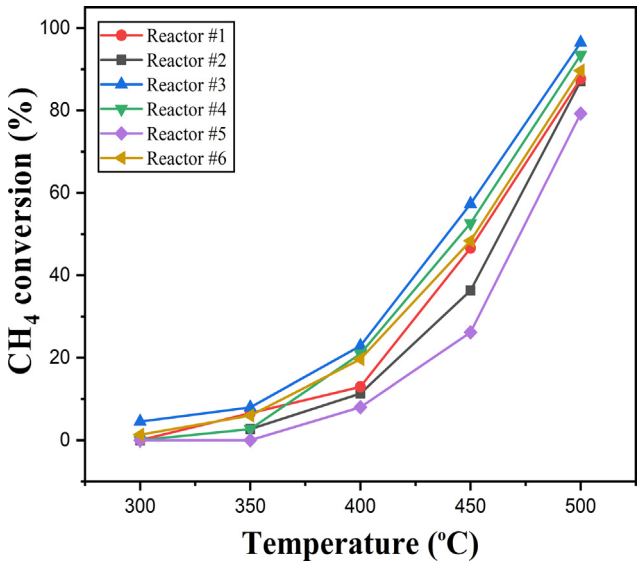

Fig. 10. Methane conversion as a function of the temperature in plate-type microreactors with different channel configurations (Reactors #1–6). Conditions: T = 300–500 °C, Φ = 6, Q_{tot} = 150 mL min^{-1}, 3.5 wt% Pt/γ-Al_2O_3 catalyst. Other reactor parameters and catalyst properties are shown in Table 1.

Table 3
T_{50} value for the CMC experimental data presented in Figs. 9a and 10.

Reactor	T_{50} (°C) [a, b]	
	Φ = 2	Φ = 6
#1	460.0	462.8
#2	451.8	456.4
#3	437.5	443.5
#4	446.0	448.4
#5	470.6	472.2
#6	449.8	452.2

[a] T_{50} indicates the temperature for reaching 50% methane conversion; Conditions are shown in Figs. 9a and 10.
[b] Estimated from the polynomial regression line (cf. other details in Table 2).

that at Φ = 6 for each channel configuration tested. In other words, the methane conversion decreased a bit when Φ increased from 2 (stoichiometric ratio) to 6 (oxygen-rich). The competitive adsorption between methane and oxygen over the catalyst surface could be one of the main reasons, given the methane adsorption energy is higher than that of oxygen (Deutschmann et al., 1996). The adsorbed oxygen is likely to inhibit the weakly adsorbed methane in these light-off experiments, leaving less chances for methane being further oxidized (Oh et al., 1992). Thus, the favorable fractional coverage of adsorbed reactants over the active sites is essential for achieving the desired methane conversion. However, caution must be taken when interpreting the trend because the difference in the T_{50} value under Φ = 2 and Φ = 6 is only several degree Celsius (cf. Table 3). An opposite trend may be observed when the operating procedures change as will be further discussed in the following sub-section.

The results of Fig. 9 were obtained in Reactors #1–6 with almost identical catalyst mass. Due to the surface area difference, the specific catalyst loading (φ) differs to some extent per reactor (Table 1). This implies a coating thickness difference, which could

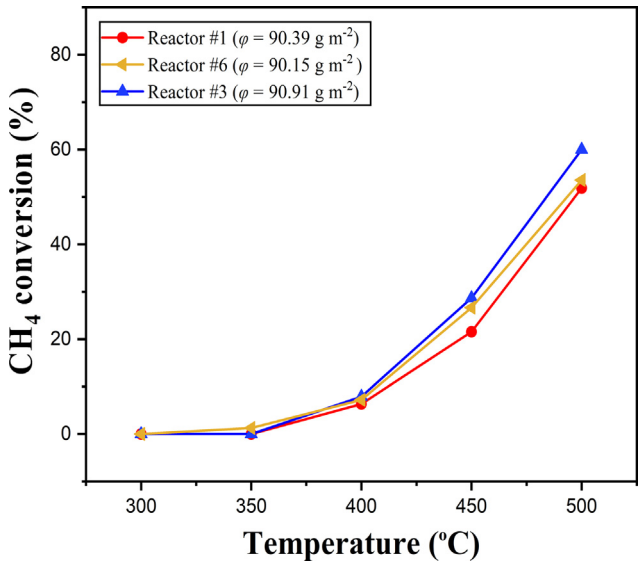

Fig. 11. Methane conversion as a function of the temperature in plate-type microreactors with different channel configurations (Reactors #1, 3 and 6). Conditions: T = 300–500 °C, Φ = 2, Q_{tot} = 300 mL min^{-1}, 3.5 wt% Pt/γ-Al_2O_3 catalyst, φ = 90.5 ± 0.5 g m^{-2} (realized by adjusting the coated catalyst mass). Other reactor parameters and catalyst properties are shown in Table 1.

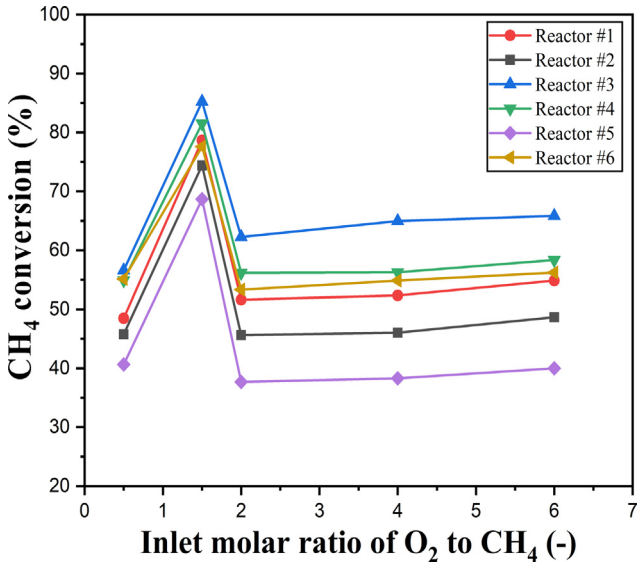

Fig. 12. Methane conversion as a function of Φ in various plate-type microreactors. Conditions: T = 450 °C, Φ = 0.5–6 (sequentially changed from small to large values in the experiments), Q_{tot} = 150 mL min^{-1}. 3.5 wt% Pt/γ-Al_2O_3, Other reactor parameters and catalyst properties are shown in Table 1.

lead to a different influence of internal diffusion on the overall reaction rate in each microreactor. To further shed light on this, some additional experiments were conducted in Reactors #1, 3 and 6, but now with almost the same specific catalyst loading (φ = 90.5 ± 0.5 g m^{-2}) by adjusting the coated catalyst mass accordingly. As shown in Fig. 11, the same conversion trend as a function of the temperature (at a total flow rate of 300 mL min^{-1} and Φ = 2) was observed in Reactors #1, #3, #6 as presented in Fig. 9b. Also, the methane conversion decrease follows the same order of Reactor #3 > Reactor #6 > Reactor #1, especially at relative higher temperatures (e.g., > 400 °C). Since in these reactors the coating thickness can be considered identical, the difference of methane conversion between each reactor is attributed to different channel geometries resulting in the different coating surface area, fluid mixing behaviour and residence time property therein.

3.2.2. Effect of molar ratio of O_2 to CH_4

To investigate the effect of the inlet molar ratio of O_2 to CH_4 (Φ), the CMC experiments were further conducted in Reactors #1–6 at 450 °C and 150 mL min^{-1}. The results of different reactors are shown in Fig. 12, which reveal the same trend in terms of the microreactor performance rank as that shown in Fig. 9a. As Φ was increased from 0.5 up to 1.5, the methane conversion was improved gradually in each microreactor, which is due to the (severely) insufficient supply of oxygen limiting the adsorbed methane to be further converted. A relatively smaller difference in methane conversion presented in this region between different microreactors compared to that of $\Phi \geq 1.5$, and the (external) mass transfer showed a more pronounced effect. The highest methane conversion was found at ca. Φ = 1.5 (instead of 2 as the stoichiometric ratio for the methane combustion) for each tested channel configuration. Oh et al. (Oh et al., 1991) also reported that operating at methane-rich conditions provided the best catalyst performance and increasing the oxygen concentration resulted in a sharp decrease in the catalyst activity. It could be thus due to firstly at Φ = 1.5, there is an increased oxygen supply together with the consumption of methane in not only the combustion reaction, but also side reactions (such as methane partial oxidation and steam reforming) that require less amount of oxygen (Bugosh et al., 2015). Moreover, a higher light-off temperature is required for the above-mentioned side reactions than for the methane combustion (Delgado et al., 2015). Such side reactions are more favoured to occur at higher temperature levels (e.g., at 450 °C relevant to Fig. 12). The existence of a variety of complex reactions under oxygen-lean conditions can be confirmed by the selectivities of CO_2, CO and H_2 as displayed in Fig. 13. For $\Phi \geq 2$, only CO_2 could be found as product (S_{CO_2} = 100%) while no CO or H_2 was detected in the product gas. For $\Phi < 2$, more amounts of CO and H_2 were produced, i.e., the selectivity of CO is ca. 2%–4% and H_2 ca. 4%–16% while the rest product is CO_2. Moreover, it seems that a balance between the adsorbed oxygen and methane has been achieved on the catalyst surface at ca. Φ = 1.5 for the best methane conversion, which largely explains the significant conversion drop at Φ = 2 or above. A way to further increase the methane conversion

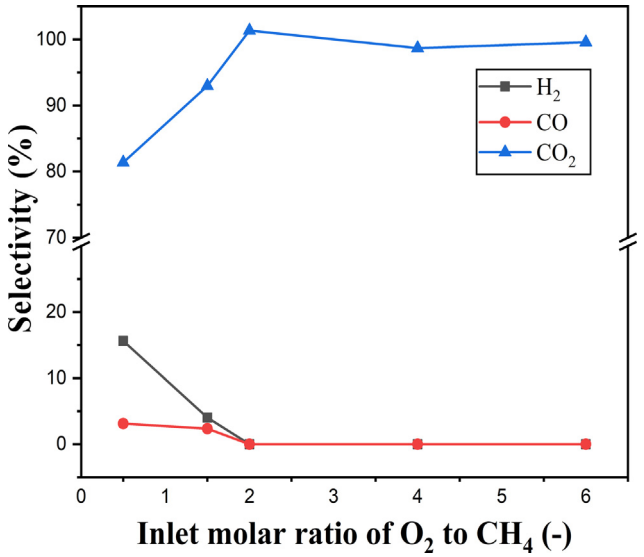

Fig. 13. Selectivities of H_2, CO, CO_2 as a function of Φ in the straight parallel channel microreactor (Reactor #1). Other conditions are the same as in Fig. 12.

(e.g., to above 90%) at this stoichiometric ratio is by raising the reaction temperature (e.g., see Fig. 9a).

In our experiments, the proportion of CO_2 in the product at ca. Φ = 1.5 is too high to achieve a desirable synthesis gas ratio of H_2/CO. It might be due to the reactant ratio and the catalyst used in this study that result in the overoxidation of products. The effects of the reactant ratio, pressure, temperature and mechanisms on the product selectivity have been evaluated in many earlier studies (York et al., 2003; Diehm and Deutschmann, 2014; Schwiedernoch et al., 2003), but additional works remain to be performed in this respect for the purpose of syngas production by catalytic methane partial oxidation.

With Φ increasing from 2 to 6, the hysteresis effect plays an important role in determining the reaction conversion. The concentration hysteresis phenomenon has been demonstrated via switching the molar ratio of O_2 to CH_4 (Amin et al., 2014; Pakharukov et al., 2015). That is, a (relatively) high conversion state has been previously obtained at Φ = 0.5–1.5 could be maintained to some extent when further increasing the Φ value afterwards. Under such circumstances, the catalyst surface was primarily dominated by the adsorbed oxygen over the catalyst surface, and the oxygen concentration on the catalyst could be considered as constant in the present molar ratio experiment due to high conversion state. Given the less methane present in the feed and competing for a constant number of active sites, relatively more methane had the possibility to be adsorbed and converted, leading to a slight conversion increase at Φ > 2.

To further elucidate the observed conversion trend especially at Φ > 2, Table 4 compares the methane conversion in the light-off experiment (Figs. 9a and 10) and that in the molar ratio experiment here (Fig. 12) under the same working conditions. The results show that the methane conversion displayed a slightly decrease as increasing O_2/CH_4 molar ratio, and on the contrary, the methane conversion turned out to be consistently higher in the molar ratio experiment. In the light-off experiment, as the experiment has been performed by increasing the temperature from 300 °C to 500 °C at a constant O_2/CH_4 molar ratio, the concentration hysteresis phenomenon is thus absent when switching from the low temperature (low conversion state) to high temperature (high conversion state). The favorable coverage between the adsorbed methane and oxygen has been achieved at Φ = 2, and the lower methane conversion at oxygen-rich environment (Φ = 6) could be reasonably explained by the competitive adsorption. The adsorbed oxygen could prevent the further oxidation of adsorbed methane over the catalyst surface due to the lower oxygen adsorption energy (Deutschmann et al., 1996). However, in the molar ratio experiment, a higher methane conversion obtained at Φ = 6 can be explained by the concentration hysteresis phenomenon present (procedurally/prehistorically related), as explained above.

Table 4
Comparison of the methane conversion in different reactors between the light-off experiment and the molar ratio experiment.

Reactor	X_{CH_4} in light-off experiment (%) [a]		X_{CH_4} in molar ratio experiment (%) [b]	
	Φ = 2	Φ = 6	Φ = 2	Φ = 6
#1	38.6	36.3	45.6	48.7
#2	48.4	46.6	51.6	54.9
#3	60.4	57.3	62.3	65.8
#4	54.8	52.6	56.2	58.4
#5	28.6	26.2	37.7	40.0
#6	52.1	48.4	53.3	56.2

[a] Conditions are shown in Fig. 9a and 10, T = 450 °C.
[b] Conditions are shown in Fig. 12.

Table 5
Comparison of ascending temperature and descending temperature procedures in CMC.

	X_{CH_4} in ascending temperature procedure [a] (%)	X_{CH_4} in descending temperature procedure [b] (%)
300 °C	0.00	14.86
400 °C	22.04	40.23

Note:
[a] Data from Fig. 9, ascending temperature operation, reactor #1, Q_{tot} = 150-mL min^{-1}, Φ = 2, 3.5 wt% Pt/γ-Al_2O_3 catalyst.
[b] Descending temperature operation, naturally cooling down, other conditions the same as ascending temperature operation.

Furthermore, based on the study of Pakharukov et al. (Pakharukov et al., 2015), it could be further explained by the difference in Pt electronic state of Pt/γ-Al_2O_3 catalyst, which is attributed to variation in O/Pt surface ratio caused by changing the oxygen concentration. It has been demonstrated (Chin et al., 2011; García-Diéguez et al., 2012) that the C—H bond activation over the oxygen-depleted Pt surface (bare Pt or O*-Pt pair sites), compared to the oxygen-covered Pt surface (O*-O* pair sites), will lead to the remarkable increase in the catalyst activity for the methane conversion.

The hysteresis effect has been supposed to first activate catalyst by varying catalyst prehistory (e.g., O_2 concentration, reaction temperature) in order to achieve the ignition, and subsequently to maintain the high conversion rate when switching back to the low conversion regime (Amin et al., 2014). In addition to the concentration hysteresis, the temperature hysteresis effect has also been observed in our experiments. Table 5 compares the CMC performance of Reactor #1 between the ascending temperature (ignition process) and the descending temperature procedure (extinction process). Methane conversion being higher during the extinction process than that during ignition process has been observed. Furthermore, the higher conversion state has been first triggered at the higher temperature (e.g., above 450 °C) and can still be maintained even after switching to the low temperature (e.g., 300 °C), clearly showing that the catalytic activity is not identical during the ignition or extinction process. This observation is

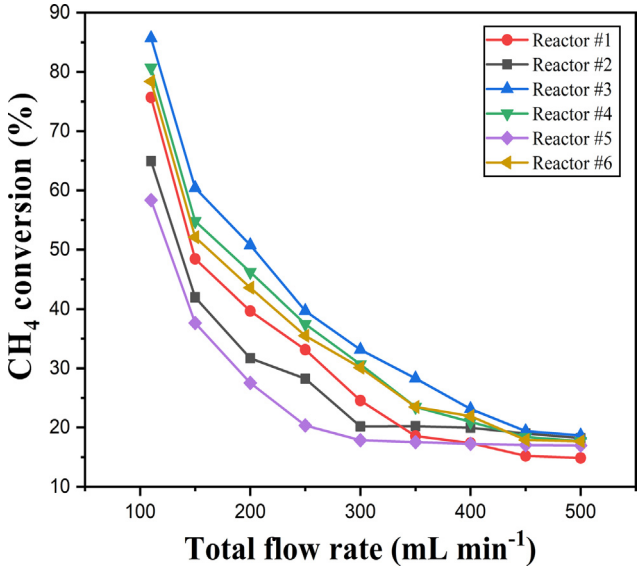

Fig. 14. Methane conversion as a function of the total gas flow rate in various plate-type microreactors. Conditions: T = 450 °C, Φ = 2, 3.5 wt% Pt/γ-Al_2O_3. Other reactor parameters and catalyst properties are shown in Table 1.

in line with the literature (Amin et al., 2014; Chen et al., 2018; Abedi et al., 2012; Raj et al., 2015), providing an alternative approach to take advantage of heat released from the reaction.

3.2.3. Effect of total flow rate

The methane conversion as a function of the total flow rate in various plate-type microreactors (Reactors #1–6) is further displayed in Fig. 14. Generally, the methane conversion remarkably decreased when the total flow rate increased, mainly due to the decreased mean residence time (τ; cf. Eq. (4)) in every tested reactor. With the increased flow rate, the methane conversion decrease tended to slow down and became insignificant especially at sufficiently high flow rates (ca. 300 mL min^{-1} for Reactors #1 and 5; ca. 450 mL min^{-1} for Reactors #2–4 and 6). This could be due to the (much) improved external mass transfer at such high flow rates that contributed positively to the methane conversion. To improve the conversion at such high flow rates, the catalyst loading/mass and/or the operating temperature should be increased, so that the kinetic rate increases and contributes more to the overall reaction rate.

4. Conclusions and prospects

An experimental investigation has been firstly performed for the CMC in the straight parallel channel microreactor (made of FeCrAlloy) with washcoated Pt/γ-Al_2O_3 catalyst. At increasing operating temperature, a remarkable increase in the methane conversion was observed. An obvious decrease in the methane conversion was found upon increasing the total flow rate due to the reduction of the residence time, and such conversion decrease is insignificant at sufficiently high flow rates due to the improved external mass transfer. The existence of an optimal catalyst specific loading (φ = 57.6 g m^{-2}) rendering the highest methane conversion has been observed. A higher specific loading (e.g., φ = 90.39 g m^{-2}) hinders the mass transfer due to a more significant internal diffusion limitation in the thicker coating layer, whereas a lower specific loading (e.g., φ = 39.45 g m^{-2}) could not provide sufficient active sites, both leading to a lower methane conversion. In this type of microreactor, the bifurcated tree-like structural component placed at the outlet as the gas collector presented a higher methane conversion than that using it as the inlet gas distributor. This could be attributed to the presence of a more uniform gas distribution in the former case.

Other five type of microreactors with different channel configurations (comprising cavity, double serpentine microchannels, obstacled microchannels, meshed circuit and vascular network) have also been tested. Their performance in the CMC has been compared with that of the straight parallel channel microreactor, with regard to the influence of various factors including the reaction temperature, inlet molar ratio of O_2 to CH_4 and total flow rate. The results suggest that the double serpentine channel microreactor exhibited the highest methane conversion, whereas the meshed circuit microreactor showed the lowest conversion. The effective usage of the coating surface area, a more uniform flow distribution and the sufficient residence time are essential factors that contribute to the higher methane conversion. A higher methane conversion was obtained in the molar ratio experiment than that in the light-off experiment under otherwise identical conditions, mainly due to the concentration hysteresis phenomenon. The highest methane conversion can be achieved in each microreactor at Φ = 1.5, because of the additional involvement of other complex side reactions under oxygen-lean conditions. The methane conversion for each tested reactor has appeared to decrease with the total gas flow rate increase due to the reduced residence time, despite the gradually improved external mass transfer.

Moreover, the partial methane oxidation under molar ratios of O_2:CH_4 < 2 has been briefly mentioned in this paper, over the same Pt/γ-Al_2O_3 catalyst. The carbon deposition over the catalyst mainly due to thermal decomposition of CH_4 and CO at high temperatures will easily result in the catalyst deactivation. Special attention is needed on the influence of different CH_4/O_2 ratios on the product selectivity distribution for downstream processes, such that an H_2/CO ratio of 2 is favorable for further methanol synthesis.

In addition, a close investigation into the fluid distribution and temperature characteristics in different channel configurations of the plate-type microreactor using CFD simulation or optical visualization techniques could be the next research step to further elucidate the reaction performance. Better understanding of the conjugated transport phenomena and more experimental data available would be beneficial to develop new mathematic models predicting the CMC performance in microreactors.

This study is expected to provide useful guidelines regarding the optimal channel configurations in plate-type microreactors for the CMC, in view of future scaling-up in practice. Some difficulties remain to be overcome for the industrial application of CMC by using microreactors. Firstly, the catalyst stability (without detachment) in the microchannel and the selection of substrate material are the requirements related to specific industrial application. Secondly, extending the catalyst lifetime (especially for noble metal as active component) is particularly essential to improve the cost-effectiveness of the CMC technology. More in-depth investigations for catalyst regeneration and replacement methods are therefore needed. Finally, more efficient reaction heat recovery is subject to further studies in order to improve the global energy efficiency of the CMC system, for instance, the CMC coupling with endothermic reactions.

CRediT authorship contribution statement

Li He: Methodology, Validation, Investigation, Writing - original draft, Writing - review & editing. **Yilin Fan:** Methodology, Validation, Writing - review & editing. **Jérôme Bellettre:** Supervision, Conceptualization, Writing - review & editing, Funding acquisition. **Jun Yue:** Supervision, Conceptualization, Writing - review & editing, Funding acquisition. **Lingai Luo:** Conceptualization, Resources, Supervision, Project administration.

Declaration of Competing Interest

The authors declare that they have no known competing financial interests or personal relationships that could have appeared to influence the work reported in this paper.

Acknowledgements

This work was supported by the Region Pays de la Loire (Chaire Connect Talent ODE) from French side; and the Ubbo-Emmius Fund 2015 from the University of Groningen and the start-up package in the area of green chemistry and technology (for Jun Yue) from the Netherlands' side. The authors thank the technical support from Gwenaël Biotteau and Nicolas Lefevre at the University of Nantes, Erwin Wilbers, Marcel de Vries, Léon Rohrbach and Daniël Vreugdenhil at the University of Groningen.

Appendix A

A.1. Design and sizing of the inlet fluid distributor and outlet fluid collector structures

The design of tree-like bifurcated structure is based on the literature (Li et al., 2008; Liu and Li, 2013), and the detailed configuration is presented in Fig. A.1a. The gas mixture flows through the cascade bifurcations, allowing a (uniform) splitting into the downstream channels. The sharp fillet structures were designed, but it tends to be the concentric fillet structure in actual plate-type multichannel reactors due to the manufacture limitation. It is reported that flow separation and recirculation could occur in the sharp fillet structure, and the concentric fillet structure without backflow is recommended (Liu et al., 2015). The detailed geometric parameters of the tree-like bifurcation are presented in Table A.1. The design of channel width at the index j (w_j) is based on the following equation:

$$w_j = w_n / r^{n-j} \tag{A.1}$$

where r is equal to 0.77 and w_n (width of the channel at the last index n) is equal to 1.50 mm (Liu and Li, 2013). The calculation of $l_{j,tot}$ (channel length between indices j and j + 1) is based on the equation:

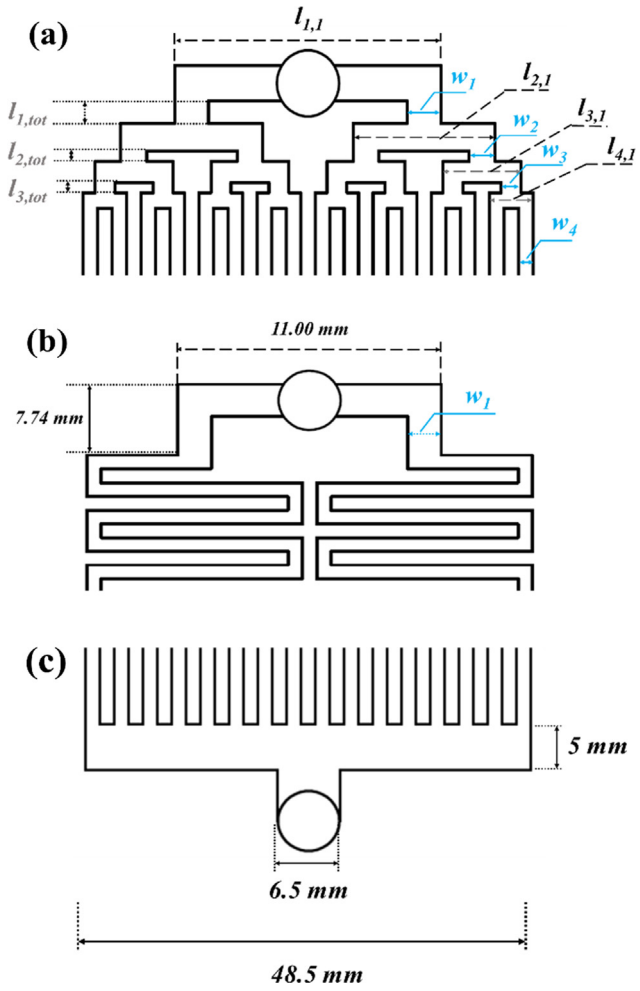

Fig. A.1. Geometry and dimensions of the inlet/outlet structures: (a) the inlet distributor for Reactors #1, 2, 4 and 5; (b) the inlet distributor and outlet collector for Reactors #3 and 6; (c) the outlet collector for Reactors #1, 2, 4 and 5.

Table A.1
Geometric parameters of tree-like bifurcated structure.

Index number j	w_j (mm)	$l_{j,tot}$ (mm)	w_j/w_{j-1} (–)	$l_{j,tot}/w_j$ (–)	$l_{j,1}$ (mm)	Re_j [a] (–)
Index 1	3.48	3.25	0.77	0.93	27.48	18.64
Index 2	2.68	1.52	0.77	0.57	14.68	11.35
Index 3	2.06	0.70	0.77	0.34	8.06	6.82
Index 4	1.50	0.30	0.73	0.20	4.50	4.03

Note:
[a] Re_j value is based on a total flow rate of 300 mL min^{-1}.

$$l_{j,tot}/w_j = 0.05 Re_j \tag{A.2}$$

where Re_j is the Reynolds number at each index j and calculated as

$$Re_j = \frac{\rho \times \frac{Q_{tot}/2^j}{w_j h} \times \frac{2hw_j}{(h+w_j)}}{\mu} \tag{A.3}$$

Thus, there is

$$Re_{j+1}/Re_j = \frac{1}{2} \frac{h + w_n/r^{n-j}}{(h + w_n/r^{n-j-1})} \tag{A.4}$$

In order to save more space for the reaction microchannel, a simple rectangular structure was utilized as the gas collector for Reactors #1, 2, 4 and 5, with its dimensions presented in Fig. A.1c. Simple bilateral divergent/convergent channels (Fig. A.1b) were used for both the inlet and outlet structures of Reactors #3 and 6.

References

Abedi, A., Hayes, R., Votsmeier, M., Epling, W.S., 2012. Inverse hysteresis phenomena during CO and C_3H_6 oxidation over a Pt/Al_2O_3 catalyst. Catal. Lett. 142, 930–935.

Ahmad, F., Silva, E.L., Varesche, M.B.A., 2018. Hydrothermal processing of biomass for anaerobic digestion-A review. Renew. Sust. Energ. Rev. 98, 108–124.

Amin, A., Abedi, A., Hayes, R., Votsmeier, M., Epling, W., 2014. Methane oxidation hysteresis over Pt/Al_2O_3. Appl. Catal. A. 478, 91–97.

Beck, I.E., Bukhtiyarov, V.I., Pakharukov, I.Y., Zaikovsky, V.I., Kriventsov, V.V., Parmon, V.N., 2009. Platinum nanoparticles on Al_2O_3: Correlation between the particle size and activity in total methane oxidation. J. Catal. 268, 60–67.

Bhagiyalakshmi, M., Anuradha, R., Park, S.D., Park, T.S., Cha, W.S., Jang, H.T., 2010. Effect of bimetallic Pt-Rh and trimetallic Pt-Pd-Rh catalysts for low temperature catalytic combustion of methane. Bull. Korean Chem. Soc. 31, 120–124.

Bugosh, G.S., Easterling, V.G., Rusakova, I.A., Harold, M.P., 2015. Anomalous steady-state and spatio-temporal features of methane oxidation on $Pt/Pd/Al_2O_3$ monolith spanning lean and rich conditions. Appl. Catal. B. 165, 68–78.

Burch, R., Loader, P.K., 1994. Investigation of Pt/Al_2O_3 and Pd/Al_2O_3 catalysts for the combustion of methane at low concentrations. Appl. Catal. B. 5, 149–164.

Cebollada, P.A.R., Garcia Bordejé, E., 2009. Optimisation of physical properties of γ-alumina coating microreactors used for the growth of a carbon nanofiber layer. Chem. Eng. J. 149, 447–454.

Chen, J., Arandiyan, H., Gao, X., Li, J., 2015. Recent advances in catalysts for methane combustion. Catal. Surv. Asia. 19, 140–171.

Chen, L., McCann, J.P., Tait, S.L., 2018. A re-examination of the catalyst activation and temperature hysteresis in methane combustion on Pt/Al_2O_3. Appl. Catal. A. 549, 19–30.

Chin, Y.-H., Buda, C., Neurock, M., Iglesia, E., 2011. Reactivity of chemisorbed oxygen atoms and their catalytic consequences during CH_4-O_2 catalysis on supported Pt clusters. J. Am. Chem. Soc. 133, 15958–15978.

Ciuparu, D., Altman, E., Pfefferle, L., 2001. Contributions of lattice oxygen in methane combustion over PdO-Based catalysts. J. Catal. 203, 64–74.

Cruellas, A., Melchiori, T., Gallucci, F., van Sint Annaland, M., 2017. Advanced reactor concepts for oxidative coupling of methane. Catal. Rev. 59, 234–294.

Delgado, K.H., Maier, L., Tischer, S., Zellner, A., Stotz, H., Deutschmann, O., 2015. Surface reaction kinetics of steam-and CO_2-reforming as well as oxidation of methane over nickel-based catalysts. Catalysts. 5, 871–904.

Deutschmann, O., Schmidt, R., Behrendt, F., Warnat, J., 1996. Numerical modeling of catalytic ignition. Symp. (Int.) Combust. 26, 1747–1754.

Diehm, C., Deutschmann, O., 2014. Hydrogen production by catalytic partial oxidation of methane over staged Pd/Rh coated monoliths: Spatially resolved concentration and temperature profiles. Int. J. Hydrogen Energy. 39, 17998–18004.

Dong, Q., Zhang, S., Duan, Z., Zhou, Q., 2006. An energy analysis of the catalytic combustion burner. Heat. Technol. Energy Eff.

Eigenberger, G., 2009. Fixed Bed Reactors. Universitätsbibliothek der Universität Stuttgart.
Exchangers, M.H., 2000. Microreactors: New Technology for Modern Chemistry. Wiley/VCH, Weinheim.
Fan, Y., Boichot, R., Goldin, T., Luo, L., 2008. Flow distribution property of the constructal distributor and heat transfer intensification in a mini heat exchanger. AlChE J. 54, 2796–2808.
Farrauto, R.J., 2012. Low-temperature oxidation of methane. Science 337, 659–660.
Farrauto, R.J., Kennelly, T., Waterman, E.M., Hobson, Jr M.C., 1993. Process conditions for operation of ignition catalyst for natural gas combustion. Google Patents.
Farrauto, R.J., Hobson, M., Kennelly, T., Waterman, E., 1992. Catalytic chemistry of supported palladium for combustion of methane. Appl. Catal. A. 81, 227–237.
Fogler, H.S., 2013. Elements of Chemical Reaction Engineering. Pearson Higher Education & Professional Group.
Ganley, J., Riechmann, K., Seebauer, E.G., Masel, R., 2004a. Porous anodic alumina optimized as a catalyst support for microreactors. J. Catal. 227, 26–32.
Ganley, J.C., Seebauer, E.G., Masel, R.I., 2004b. Porous anodic alumina microreactors for production of hydrogen from ammonia. AlChE J. 50, 829–834.
Garbowski, E., Feumi-Jantou, C., Mouaddib, N., Primet, M., 1994. Catalytic combustion of methane over palladium supported on alumina catalysts: Evidence for reconstruction of particles. Appl. Catal. A. 109, 277–291.
García-Diéguez, M., Chin, Y.-H.C., Iglesia, E., 2012. Catalytic reactions of dioxygen with ethane and methane on platinum clusters: Mechanistic connections, site requirements, and consequences of chemisorbed oxygen. J. Catal. 285, 260–272.
Gélin, P., Primet, M., 2002. Complete oxidation of methane at low temperature over noble metal based catalysts: a review. Appl. Catal. B. 39, 1–37.
Giani, L., Cristiani, C., Groppi, G., Tronconi, E., 2006. Washcoating method for Pd/γ-Al_2O_3 deposition on metallic foams. Appl. Catal B. 62, 121–131.
Gielen D., 2018. Global energy transformation - a roadmap to 2050, International Renewable Energy Agency (IRENA).
Guo, X., Fan, Y., Luo, L., 2014. Multi-channel heat exchanger-reactor using arborescent distributors: A characterization study of fluid distribution, heat exchange performance and exothermic reaction. Energy. 69, 728–741.
Haas-Santo, K., Fichtner, M., Schubert, K., 2001. Preparation of microstructure compatible porous supports by sol-gel synthesis for catalyst coatings. Appl. Catal. A. 220, 79–92.
Halabi, M., De Croon, M., Van Der Schaaf, J., Cobden, P., Schouten, J., 2010. Intrinsic kinetics of low temperature catalytic methane-steam reforming and water-gas shift over $Rh/Ce_xZr_{1-x}O_2$ catalyst. Appl. Catal. A. 389, 80–91.
Hao, H., Liu, Z., Zhao, F., Li, W., 2016. Natural gas as vehicle fuel in China: A review. Renew. Sust. Energ. Rev. 62, 521–533.
He, L., Fan, Y., Bellettre, J., Yue, J., Luo, L., 2019. A review on catalytic methane combustion at low temperatures: Catalysts, mechanisms, reaction conditions and reactor designs. Renew. Sust. Energ. Rev., 109589
He, L., Fan, Y., Luo, L., Bellettre, J., Yue, J., 2020. Preparation of Pt/γ-Al_2O_3 catalyst coating in microreactors for catalytic methane combustion. Chem. Eng. J. 380, 122424.
Hwang, C.-P., Yeh, C.-T., 1999. Platinum-oxide species formed on progressive oxidation of platinum crystallites supported on silica and silica-alumina. J. Catal. 182, 48–55.
Jensen, K.F., 2001. Microreaction engineering-is small better? Chem. Eng. Sci. 56, 293–303.
Jodłowski, P., Jędrzejczyk, R., Chlebda, D., Dziedzicka, A., Kuterasiński, Ł., Gancarczyk, A., Sitarz, M., 2017. Non-noble metal oxide catalysts for methane catalytic combustion: sonochemical synthesis and characterisation. Nanomaterials. 7, 174.
Karavalakis, G., Durbin, T.D., Villela, M., Miller, J.W., 2012. Air pollutant emissions of light-duty vehicles operating on various natural gas compositions. J Nat. Gas Sci. Eng 4, 8–16.
Lee, J.H., Trimm, D.L., 1995. Catalytic combustion of methane. Fuel Process. Technol. 42, 339–359.
Li, P., Coopamah, D., Dhar, N., 2008. Analysis and optimization of flow distribution channels for uniform flow in fuel cells. In: ASME 2008 Fluids Engineering Division Summer Meeting collocated with the Heat Transfer, Energy Sustainability, and 3rd Energy Nanotechnology Conferences. American Society of Mechanical Engineers Digital Collection.
Liauw, M., Baerns, M., Broucek, R., Buyevskaya, O., Commenge, J., Corriou, J., Falk, L., Gebauer, K., Hefter, H., Langer, O., 2000. Microreaction Technology: Industrial Prospects. Springer, pp. 224–234.
Liu, H., Li, P., 2013. Even distribution/dividing of single-phase fluids by symmetric bifurcation of flow channels. Int. J. Heat Fluid Flow. 40, 165–179.
Liu, H., Li, P., Wang, K., 2015. The flow downstream of a bifurcation of a flow channel for uniform flow distribution via cascade flow channel bifurcations. Appl. Therm. Eng. 81, 114–127.
Liu, R.H., Stremler, M.A., Sharp, K.V., Olsen, M.G., Santiago, J.G., Adrian, R.J., Aref, H., Beebe, D.J., 2000. Passive mixing in a three-dimensional serpentine microchannel. J. Microelectromech. Syst. 9, 190–197.
Lyubovsky, M., Smith, L.L., Castaldi, M., Karim, H., Nentwick, B., Etemad, S., LaPierre, R., Pfefferle, W.C., 2003. Catalytic combustion over platinum group catalysts: fuel-lean versus fuel-rich operation. Catal. Today. 83, 71–84.
Manisalidis, I., Stavropoulou, E., Stavropoulos, A., Bezirtzoglou, E., 2020. Environmental and health impacts of air pollution: a review. Frontiers. Public Health. 8.
Mehrpooya, M., Khalili, M., Sharifzadeh, M.M.M., 2018. Model development and energy and exergy analysis of the biomass gasification process (Based on the various biomass sources). Renew. Sust. Energ. Rev. 91, 869–887.
Mei, H., Li, C., Ji, S., Liu, H., 2007. Modeling of a metal monolith catalytic reactor for methane steam reforming-combustion coupling. Chem. Eng. Sci. 62, 4294–4303.
Meille, V., Pallier, S., Santacruzbustamante, G., Roumanie, M., Reymond, J., 2005. Deposition of γ-Al_2O_3 layers on structured supports for the design of new catalytic reactors. Appl. Catal. A. 286, 232–238.
Mettler, M.S., Stefanidis, G.D., Vlachos, D.G., 2010. Scale-out of microreactor stacks for portable and distributed processing: coupling of exothermic and endothermic processes for syngas production. Ind. Eng. Chem. Res. 49, 10942–10955.
Miesse, C.M., Masel, R.I., Jensen, C.D., Shannon, M.A., Short, M., 2004. Submillimeter-scale combustion. AlChE J. 50, 3206–3214.
Mills, P.L., Quiram, D.J., Ryley, J.F., 2007. Microreactor technology and process miniaturization for catalytic reactions-A perspective on recent developments and emerging technologies. Chem. Eng. Sci. 62, 6992–7010.
Müller, C.A., Maciejewski, M., Koeppel, R.A., Tschan, R., Baiker, A., 1996. Role of lattice oxygen in the combustion of methane over PdO/ZrO_2: combined pulse TG/DTA and MS study with ^{18}O-labeled catalyst. J. Phys. Chem. 100, 20006–20014.
Müller, C.A., Maciejewski, M., Koeppel, R.A., Baiker, A., 1999. Combustion of methane over palladium/zirconia: effect of Pd-particle size and role of lattice oxygen. Catal. Today. 47, 245–252.
Mundhwa, M., Thurgood, C.P., 2017. Numerical study of methane steam reforming and methane combustion over the segmented and continuously coated layers of catalysts in a plate reactor. Fuel Process. Technol. 158, 57–72.
Mundhwa, M., Parmar, R.D., Thurgood, C.P., 2017. A comparative parametric study of a catalytic plate methane reformer coated with segmented and continuous layers of combustion catalyst for hydrogen production. J. Power Sources. 344, 85–102.
Ni, Z., Seebauer, E., Masel, R.I., 2005. Effects of microreactor geometry on performance: differences between posted reactors and channel reactors. Ind. Eng. Chem. Res. 44, 4267–4271.
O'Connell, M., Kolb, G., Zapf, R., Men, Y., Hessel, V., 2009. Bimetallic catalysts for the catalytic combustion of methane using microreactor technology. Catal. Today. 144, 306–311.
Oh, S.H., Mitchell, P.J., Siewert, R.M., 1991. Methane oxidation over alumina-supported noble metal catalysts with and without cerium additives. J. Catal. 132, 287–301.
Oh, S., Mitchell, P., Siewert, R., 1992. Methane oxidation over noble metal catalysts as related to controlling natural gas vehicle exhaust emissions, Catalytic control of air pollution. ACS Publication, Washington, DC.
Pakharukov, I.Y., Stakheev, A.Y., Beck, I.E., Zubavichus, Y.V., Murzin, V.Y., Parmon, V. N., Bukhtiyarov, V.I., 2015. Concentration hysteresis in the oxidation of methane over Pt/γ-Al_2O_3: X-ray absorption spectroscopy and kinetic study. ACS Catal. 5, 2795–2804.
Pecchi, G., Reyes, P., López, T., Gómez, R., 2004. Pd-CeO_2 and Pd-La_2O_3/alumina-supported catalysts: their effect on the catalytic combustion of methane. J. Non-Cryst. Solids. 345, 624–627.
Peela, N.R., Mubayi, A., Kunzru, D., 2009. Washcoating of γ-alumina on stainless steel microchannels. Catal. Today. 147, S17–S23.
Persson, K., Ersson, A., Carrera, A.M., Jayasuriya, J., Fakhrai, R., Fransson, T., Järås, S., 2005. Supported palladium-platinum catalyst for methane combustion at high pressure. Catal. Today. 100, 479–483.
Persson, K., Jansson, K., Jaras, S., 2007. Characterisation and microstructure of Pd and bimetallic Pd-Pt catalysts during methane oxidation. J. Catal. 245, 401–414.
Petrov, A.W., Ferri, D., Krumeich, F., Nachtegaal, M., van Bokhoven, J.A., Kröcher, O., 2018. Stable complete methane oxidation over palladium based zeolite catalysts. Nat. Commun. 9, 2545–2553.
Raj, R., Harold, M.P., Balakotaiah, V., 2015. Steady-state and dynamic hysteresis effects during lean co-oxidation of CO and C_3H_6 over Pt/Al_2O_3 monolithic catalyst. Chem. Eng. J. 281, 322–333.
Ramaswamy, R.C., Ramachandran, P.A., Duduković, M.P., 2008. Coupling exothermic and endothermic reactions in adiabatic reactors. Chem. Eng. Sci. 63, 1654–1667.
Schmidt, B., Liauw, M., 2005. Mass transfer limitations in microchannel reactors. Catal. Today. 110, 15–25.
Schwiedernoch, R., Tischer, S., Correa, C., Deutschmann, O., 2003. Experimental and numerical study on the transient behavior of partial oxidation of methane in a catalytic monolith. Chem. Eng. Sci. 58, 633–642.
Seimanides, S., Stoukides, M., 1986. Catalytic oxidation of methane on polycrystalline palladium supported on stabilized zirconia. J. Catal. 98, 540–549.
Seo, Y.S., Yu, S.P., Cho, S.J., Song, K.S., 2003. The catalytic heat exchanger using catalytic fin tubes. Chem. Eng. Sci. 58, 43–53.
Specchia, S., Finocchio, E., Busca, G., Saracco, G., Specchia, V., 2009. Effect of S-compounds on Pd over $LaMnO_3{\cdot}2ZrO_2$ and $CeO_2{\cdot}2ZrO_2$ catalysts for CH_4 combustion. Catal. Today. 143, 86–93.
Su, S., Yu, X., 2015. A 25 kWe low concentration methane catalytic combustion gas turbine prototype unit. Energy. 79, 428–438.
T.V. Choudhary, S.B., Choudhary, V.R., 2002. Catalysts for combustion of methane and lower alkanes review. Appl. Catal. A. 234, 1–23.
Tondeur, D., Fan, Y., Commenge, J.-M., Luo, L., 2011. Uniform flows in rectangular lattice networks. Chem. Eng. Sci. 66, 5301–5312.
Wang, Z., Deng, J., Liu, Y., Yang, H., Xie, S., Wu, Z., Dai, H., 2017. Three-dimensionally ordered macroporous $CoCr_2O_4$-supported Au-Pd alloy nanoparticles: Highly active catalysts for methane combustion. Catal. Today. 281. Part 3, 467–476.

Wang, D., Gong, J., Luo, J., Li, J., Kamasamudram, K., Currier, N., Yezerets, A., 2019. Distinct reaction pathways of methane oxidation on different oxidation states over Pd-based three-way catalyst (TWC). Appl. Catal. A. 572, 44–50.

X. Chun D., 2005. Applied studies on methane catalytic combustion development of a natural gas premixed catalytic burner and boiler for household applications. Sichuan University. Thesis in Chinese.

Xu, X., Vonk, H., Cybulski, A., Moulijn, J.A., 1995. Alumina washcoating and metal deposition of ceramic monoliths. Stud. Surf. Sci. Catal., 1069–1078

Yang, J., Guo, Y., 2018. Nanostructured perovskite oxides as promising substitutes of noble metals catalysts for catalytic combustion of methane. Chin. Chem. Lett. 29, 252–260.

York, A.P., Xiao, T., Green, M.L., 2003. Brief overview of the partial oxidation of methane to synthesis gas. Top. Catal. 22, 345–358.

Zapf, R., Becker-Willinger, C., Berresheim, K., Bolz, H., Gnaser, H., Hessel, V., Kolb, G., Löb, P., Pannwitt, A.K., Ziogas, A., 2003. Detailed characterization of various porous alumina-based catalyst coatings within microchannels and their testing for methanol steam reforming. Chem. Eng. Res. Des. 81, 721–729.

Zhou, P., Tarlet, D., Fan, Y., Hu, X., Luo, L., 2018. Water-in-oil emulsification in a bifurcated tree-like network: Flow distribution properties and their impact on the emulsion polydispersity. Chem. Eng. Res. Des. 134, 420–433.

Zou, C., Zhao, Q., Zhang, G., Xiong, B., 2016. Energy revolution: from a fossil energy era to a new energy era. Nat. Gas Ind. B. 3, 1–11.